Supporting Information

Molybdenum-maltolate as a Molybdopterin Mimic for Bioinspired Oxidation Reaction

Swapnil S. Pawar,[a] Rohit N. Ketkar,[a] Pranav B. Gaware,[a] Kaustubh U. Jagushte,[a] Divyani Dhawne,[a] Shreyada N. Save,[b] Shilpy Sharma,[b] Ganga Periyasamy,[c] Niyamat Chimthanawala,[d] Sadhana Sathaye,[d] Prof. Shreerang V. Joshi,[d] Nabanita Sadhukhan,*[a]

[a]Department of Speciality Chemicals Technology, Institute of Chemical Technology, N.P. Marg, Matunga, Mumbai, Maharashtra - 400019, INDIA.
[b]Department of Biotechnology, Savitribai Phule Pune University, Ganeshkind Rd, Pune, Maharashtra – 411007, INDIA.
[c]Department of Chemistry, Central College Campus, Bangalore University, Bangalore 560001, INDIA
[d]Department of Pharmaceutical Sciences and Technology, Institute of Chemical Technology, N.P. Marg, Matunga, Mumbai, Maharashtra - 400019, INDIA.

*To whom correspondence should be addressed.

Email address: nn.sadhukhan@ictmumbai.edu.in

Table of Contents

		Page No.
1.	**General Information**	**S4**
2.	**Synthetic procedures**	**S5**
3.	**Figures and Tables**	**S7**
	Fig. S1. ATR–FTIR spectra of **Maltol** and **[$MoO_2(Mal)_2$]**.	**S7**
	Fig. S2. ESI–MS of **Maltol.**	**S8**
	Fig. S3. ESI–MS of **[$MoO_2(Mal)_2$]**.	**S8**
	Fig. S4. Stacked ^{13}C NMR spectra of **Maltol** and **[$MoO_2(Mal)_2$]**.	**S9**
	Fig. S5 Thermogravimetric analysis (TGA) of **[$MoO_2(Mal)_2$]**.	**S9**
	Table S1. Crystallographic data and structure refinement for **Maltol.**	**S10**
	Fig. S6. ORTEP diagram of **Maltol** in 50% occupancy.	**S10**
	Table S2. Bond lengths for **Maltol**.	**S11**
	Table S3. Bond angles for **Maltol**.	**S13**
	Table S4. Crystallographic data and structure refinement for complex 1 **[$MoO_2(Mal)_2$]**.	**S16**
	Fig. S7. ORTEP diagram of complex 1 **[$MoO_2(Mal)_2$]**.	**S16**
	Table S5. Bond lengths for complex 1 **[$MoO_2(Mal)_2$]**.	**S17**
	Table S6. Bond angles for complex 1 **[$MoO_2(Mal)_2$]**.	**S17**
4.	**[$MoO_2(Mal)_2$] catalyzed oxidation reactions**	**S19**
	Table S7. [$MoO_2(Mal)_2$] catalyzed oxidation reactions.	**S19**
	Fig. S9. GC chromatogram of oxidation of diphenylmethane catalyzed by **[$MoO_2(Mal)_2$]** using H_2O_2 as an oxidant.	**S20**
	Fig. S10. GC chromatogram of oxidation of toluene to benzaldehyde catalyzed by **[$MoO_2(Mal)_2$]** by using 1 mmol TBHP as an oxidant.	**S21**
	Fig. S11. GC chromatogram of oxidation of toluene to benzaldehyde catalyzed by **[$MoO_2(Mal)_2$]** by using 2 mmol TBHP as an oxidant.	**S22**
	Fig. S12. GC chromatogram of oxidation of toluene to benzaldehyde catalyzed by **[$MoO_2(Mal)_2$]** by using 5 mmol TBHP as an oxidant.	**S22**
	Fig. S13. GC chromatogram of oxidation of toluene to benzaldehyde catalyzed by **[$MoO_2(Mal)_2$]** by using 5 mmol TBHP as an oxidant.	**S22**
	Fig. S14. Stacked ^1H NMR spectra of toluene and its oxidation reaction mixtures at different time intervals in *dmso-d_6*.	**S23**
	Fig. S15. Stacked ATR-FTIR spectra of toluene and its oxidation reaction mixtures	**S23**
	Fig. S16. GC chromatogram of oxidation of styrene to styrene oxide catalyzed by **[$MoO_2(Mal)_2$]** by using 0.5 mmol TBHP as an oxidant.	**S24**
	Fig. S17. GC chromatogram of oxidation of hypoxanthine to xanthine catalyzed by **[$MoO_2(Mal)_2$]** by using 1 mmol TBHP as oxidant at room temperature for 15h.	**S25**
	Fig. S18. GC chromatogram of oxidation of hypoxanthine to xanthine catalyzed by **[$MoO_2(Mal)_2$]** by using 1 mmol TBHP as an oxidant at 100°C for 15 h.	**S26**
	Fig. S19. Stacked ^1H NMR spectra of xanthine, reaction mixture after 24, 9, 6, 3, 0 h, **[$MoO_2(Mal)_2$]** and hypoxanthine in *dmso-d_6* respectively.	**S26**
	Fig. S20. ESI–MS of xanthine.	**S27**
	Fig. S21. Absorption spectra of **[$MoO_2(Mal)_2$]** in the presence of NBT and TBHP in ACN at 25 °C.	**S28**
5.	**Control Studies**	**S29**
	Fig. S22. Stacked ^1H NMR spectra of the reaction mixture of hypoxanthine to xanthine in the presence of **$(NH_4)_6Mo_7O_{24}.4H_2O$** at 0 hr and 24 hr in *dmso-d_6*.	**S29**

	Fig. S23. Stacked ^{1}H NMR spectra of the reaction mixture of hypoxanthine to xanthine in the presence of **$C_{10}H_{14}MoO_6$** at 0 hr and 24 hr in *dmso-d_6*.	**S29**
	Fig. S24. Stacked ^{1}H NMR spectra of the reaction mixture of toluene to benzaldehyde in the presence of **$(NH_4)_6Mo_7O_{24}$**. $4H_2O$ at 0 hr and 24 hr *dmso-d_6*.	**S30**
	Fig. S25. Stacked ^{1}H NMR spectra of the reaction mixture of toluene to benzaldehyde in the presence of **$C_{10}H_{14}MoO_6$** at 0 hr and 24 hr in *dmso-d_6*.	**S30**
	Fig. S26. Absorption spectra of **Ammonium molybdate $(NH_4)_6Mo_7O_{24}\cdot 4\,H_2O$** in the presence of NBT and TBHP in ACN at 25 °C.	**S31**
	Fig. S27. Absorption spectra of **Bis(acetylacetonato)dioxomolybdenum(VI) [$MoO_2(acac)_2$]** in the presence of NBT and TBHP in ACN at 25 °C.	**S32**
	Fig. S29. Effect of a) maltol; and b) ammonium heptamolybdate on cell viability	**S33**
6.	**Computational Studies**	**S34**
	Fig. S28. The computed the IR frequencies for mono oxoperoxo-Molybdenum complex. The Peroxo based vibrations are highlighted in the figure.	**S34**
	Fig. S29. (a) Optimized geometry with important bond distances in Å, (b) Frontier molecular orbitals (c) Molecular electrostatic potential map (isocontour value 0.002 eV/bohr^2) and (d) the definition of dihedral angle calculation of Mo(VI) mono oxoperoxo complex.	**S34**
7.	**References**	**S36**

1. General Information

Materials and Methods

All chemicals were purchased from commercial sources and used directly without further purification. Boric acid, acetic acid, ammonium heptamolybdate, acetonitrile, ethanol, and t-butanol were purchased from Spectrochem Pvt. Ltd, India. Sodium hypochlorite solution, 30% hydrogen peroxide solution, and mesitylene were purchased from Avra Synthesis Pvt. Ltd, India. [MoO2(acac)2], 2-acetylfuran, sodium borohydride, and tert-butyl hydroperoxide 5.0 M in decane were procured from Sigma-Aldrich. Deuterated solvents were also purchased from Sigma-Aldrich. All solvents were dried before use according to the procedures reported in the literature. [1] Reactions were magnetically stirred under a nitrogen atmosphere unless otherwise stated and monitored by thin-layer chromatography (TLC) alumina sheets (Merck, USA), and were visualized by observation under UV light (254 nm). Volatile solvents were removed via distillation at the appropriate temperature and pressure. 1-(2-furyl) ethanol[2] and t-butyl hypochlorite[3] were synthesized according to a reported procedure. A Bruker ALPHA-II spectrophotometer was used for recording IR Spectra. An Agilent USA Technologies 400 MHz spectrometer was used for measuring ^{1}H and ^{13}C NMR Spectra where $CDCl_3$ and *dmso-*d_6 were used as the internal standard. ESI-MS was recorded on an Advion-Plate Express instrument (USA) operating in ESI-Mode. The Thermogravimetric analysis (TGA) was done on a Hitachi STA7300 Thermal Analysis System. CV and DPV were performed under the electrochemical workstation. The UV-visible absorption spectra were recorded on a Jasco-V-750, Japan spectrophotometer. Gas chromatography analysis was carried out using Agilent Technologies 7890 B network GC System, equipped with an Agilent Technologies G4513A series autosampler and a glass capillary HP-5, ID: 0.32 mm, length: 30 m, film thickness: 0.25 µm; packed with non-polar polymer [(5%-phenyl)-methylpolysiloxane. The single-crystal XRD data was collected by selecting and placing a suitable crystal on a dtrek-CrysAlisPro-abstract goniometer imported rigaku-d*trek images diffractometer (USA). The crystal was kept at 150 K during data collection. Using Olex2 [1], the structure was solved with the ShelXT [2] structure solution program using Intrinsic Phasing and refined with the ShelXL [3] refinement package using Least Squares minimization. The structure was optimized using the CAM-B3LYP long range corrected hybrid functional, as implemented in the Gaussian 09 suite of programs, with the Los Alamos effective core potential and basis set on Mo (LANL2DZ) and the 6-31+G(d,p) basis set on all other atoms.[4] The computed all real harmonic vibrational frequencies confirm the minima nature of the geometry. All animal studies were ethically reviewed and carried out in accordance with the Committee for the Purpose of Control and Supervision of Experiments on Animals (CPCSEA) Institutional Animal Ethics Committee (IAEC) following acute oral toxicity (OECD) 420 guidelines (IAEC/ICT/2022/P20).

Cell culture

Non-cancerous cell lines namely, mouse embryonic fibroblasts (MEFs & NIH-3T3), human embryonic kidney (HEK293T) cells; and cancerous cell lines namely, MCF7 (human breast cancer), A549 (human alveolar basal epithelial cells) cells were grown in high glucose Dulbecco's modified Eagle medium (DMEM; ThermoFisher Scientific) containing 10% heat-inactivated fetal bovine serum (FBS; ThermoFisher Scientific) and 100 units/ml penicillin and 100 µg/ml streptomycin in humidified 5% CO_2 incubator (Thermo Scientific) at 37°C.

MTT-based cytotoxicity assay

Cellular viability in the presence of an increasing concentration of metal-organic complex $C_{16}H_{24}MoO_8$ was performed using MTT assay. Briefly, cells were dispersed in tissue-cultured treated 96-well plates (Corning) at a density of 8 x 10^4 cells/well (per 100µL) in a complete DMEM medium and were allowed to adhere at 37°C for 24 hrs. Cells were incubated with increasing concentrations of metal-organic

complex $C_{16}H_{24}MoO_8$ (1-100 µM) for 24 hrs. Post incubation, media was removed and the plates were incubated with 100 µL of MTT solution (0.5 mg/ml in PBS) at 37°C for 4 hrs. The formazan crystals, thus formed, were dissolved with 100 µL solubilization buffer (10% SDS/0.1N HCl) for 4 hrs at RT. Absorbance was measured at 570 nm using a multi-mode plate reader (Hidex). Relative cell viability was expressed as a percentage for each treatment with respect to control wells (untreated wells, set as 100 %). All experiments were repeated four times (N = 4).

Oral toxicity studies

The acute oral toxicity test was carried out for the prepared formulation $[MoO_2(Mal)_2]$ and administered to the animals in accordance with the OECD guideline 420 (fixed-dose procedure). Briefly, 20 female Swiss albino mice weighing 25 ± 2 g animals were divided into 04 groups, each group containing 05 animals. A limit test was performed with a starting dose of 2000 mg/kg and administered to a group of 05 animals. If the animal showed no mortality or morbidity, the compound was considered safe or non-toxic. This would then be followed by dosing of a further four animals at this level serving as a limit test for this guideline.

For the main study, a starting dose of 5mg/kg was administered to Group I, followed by 50 mg/kg, 300 mg/kg, and 2000 mg/kg to Group II, III, and IV, respectively. The animals were observed individually after dosing at least once during the first 30 minutes, periodically during the first 24 hours, and daily thereafter, for a total of 14 days. All animals showed no signs of toxicity. The prepared formulation was found to be safe/non-toxic.

Statistical Analysis

Statistical analysis was performed using one-way analysis of variance (ANOVA). $p < 0.05$ was considered to be statistically significant.

2. Synthetic Procedures

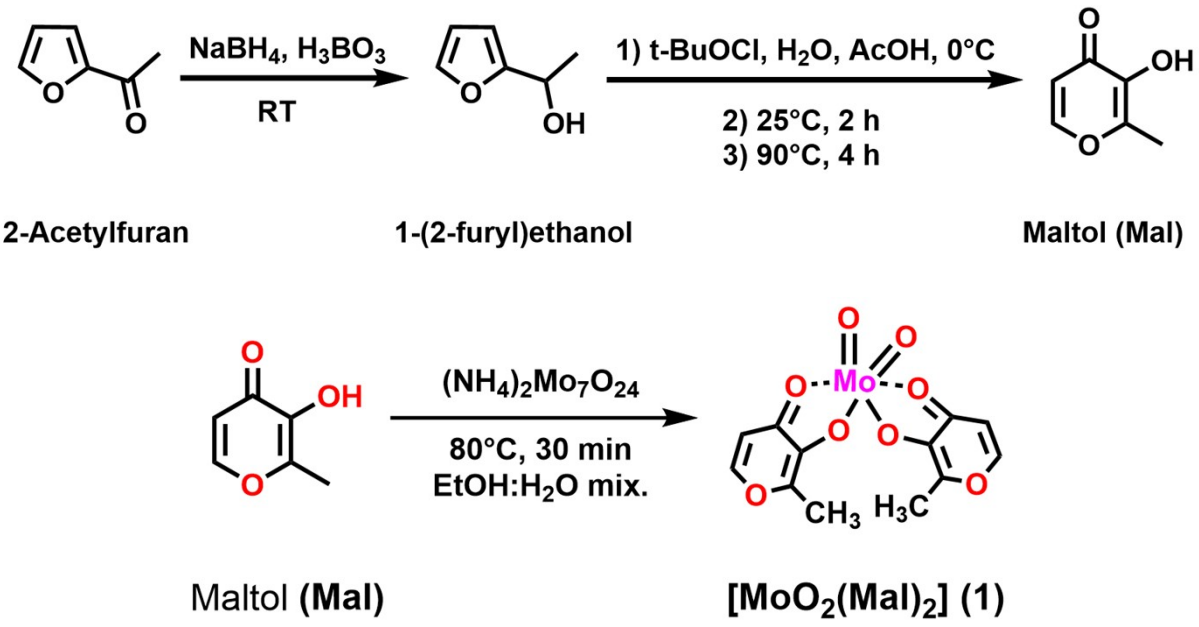

Scheme S1. Synthetic scheme for the synthesis of **Maltol** and **$[MoO_2(Mal)_2]$**.

Synthesis of Maltol (Mal):

A two neck round bottom flask equipped with a magnetic stirrer is placed and solution of 1(2-furyl ethanol) (2) (2 g, 17.83 mmol) in 35 % aquatic acetic acid (17.5 gm, 297.35 mmol) is added in a round bottom flask. The flask is placed in an ice bath and stirred at a temperature of -5 to 0°C. Then *t*-butyl hypochlorite (7.745 gm, 71.34 mmol) is gradually added to the solution by using an addition funnel. After addition, the mixture was kept at room temperature to achieve 25°C temperature. Then the stirring is continued at 25°C for the next 2 hours. The mixture was then heated at 90°C for the next 4 hours with continuous stirring. Then the reaction was stopped and the solution was neutralized by the dropwise addition of a saturated solution of $NaHCO_3$. Then the mixture was extracted by washing three times with chloroform ($CHCl_3$) and the aqueous layer is discarded. The organic layer is then evaporated and concentrated to give crystals (1.2 gm) in 61 % yield. IR (cm^{-1}): 3252 (O-H), 2974 (C-H), 1654 (C=O), 1615 (C=C), 1075 (C-O-C). ^{1}H NMR ($CDCl_3$): δ 2.34 (3H, CH_3), δ 6.39 (1H, CH), δ 7.24 (1H, O-H), δ 7.67 (1H, CH). ^{13}C NMR ($CDCl_3$): δ 173.0, δ 154.1, δ 149.2, δ 143.2, δ 113.1, δ 14.2. MS (ESI), (*m/z*) calc. for $C_6H_6O_3$ = 126.03, found: 125.4 $[M-H]^+$.

Synthesis of $[MoO_2(Mal)_2]$ complex:

In a beaker ammonium heptamolybdate $[(NH_4)_6Mo_7O_{24}\bullet 4H_2O]$ (1 g, 0.86 mmol), was dissolved in (10 mL) of warm water. Then keep it for cooling at room temperature, In another beaker maltol (0.22 gm, 1.74 mmol) was dissolved in ethanol. Then round bottom flask was equipped with a magnetic stirrer with an oil bath and the solution of ammonium heptamolybdate was added to the flask. The temperature should be at 80°C. Then the solution of Maltol and ethanol was added to the flask. Then the mixture was stirred for the next 30 minutes. After the addition of maltol ethanol solution suddenly yellow colour change is observed. After 30 minutes the mixture was filtered and washed with a hot mixture of ethanol and water and then dried at 110°C. Recrystallization of the crude from chloroform afforded yellow crystalline product **1**. The yield of the product is 60 %. Chemical characterization by ATR-FTIR, NMR (^{1}H and ^{13}C), and ESI-Mass spectroscopy, X-Ray single crystal of the complex verified their preparation. Anal. Calcd for $C_{12}H_{10}MoO_8$: C, 38.11; H, 2.67. Found: C, 38.05; H, 2.43. IR (cm^{-1}): 3071 (O-H), 1623 (C=O), 1568(C=C), 1203 (C-O-C). ^{1}H NMR ($CDCl_3$): δ 2.5 (3H, CH_3), δ 6.6 (1H, CH), δ 7.9 (1H, CH). ^{13}C NMR ($CDCl_3$): δ 154.2, δ 148.9, δ 143.2, δ 49.9, δ 29.6, δ 14.2. MS (ESI), (*m/z*) calc. for $C_{12}H_{10}MoO_8$ = 378.14, found: 379.4 $[M+H]^+$.

3. Figures and Tables

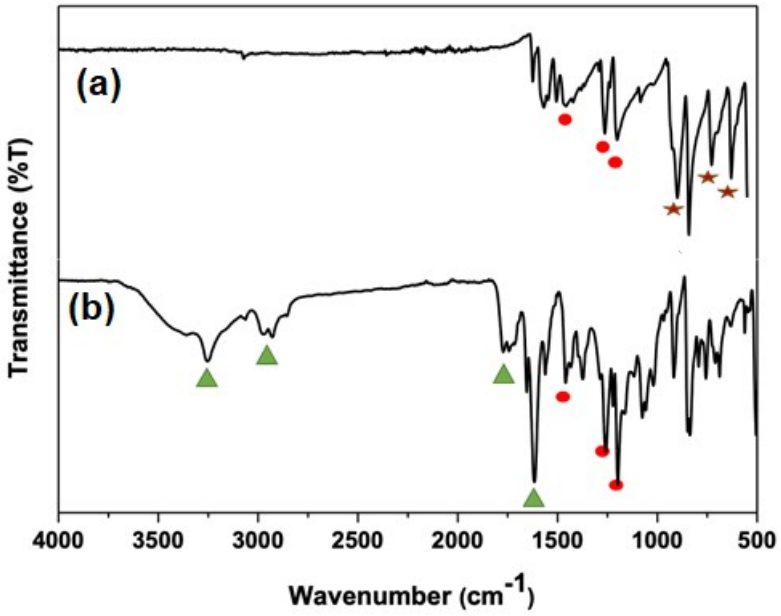

Fig. S1. ATR–FTIR spectra of (a) **[$MoO_2(Mal)_2$]** (top), (b) **Maltol** (bottom). Peak disappeared after complexation with maltol are marked with green triangle (▲) 3520 (O-H), 2974 (C-H), 1772 (C=O), 1616 (C=C); Peak intensity changed after complexation are marked with red circle (●) 1459 (C-H), 1257 (C-O), 1198 (C-O); New peaks appeared after complexations are marked with maroon star (★) 894 (Mo=O).

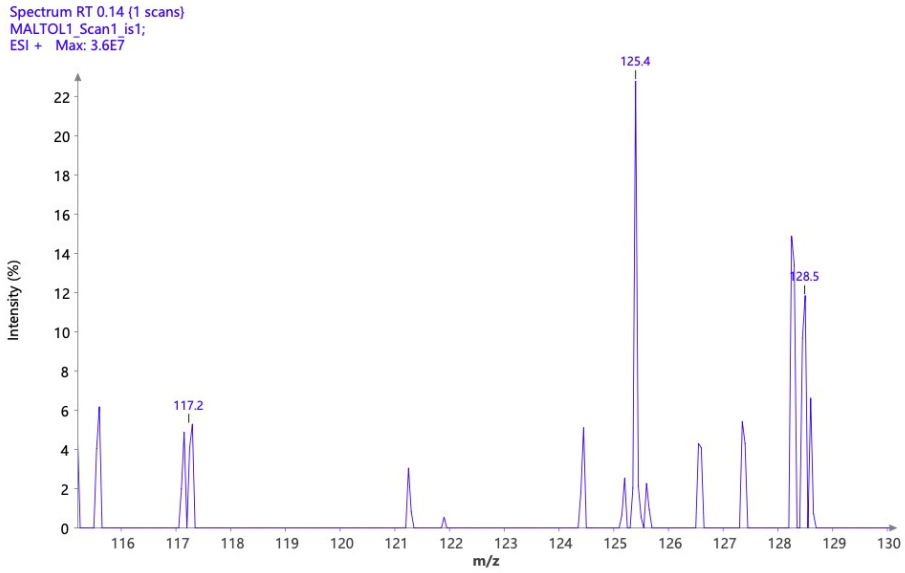

Fig. S2. ESI–MS of **Maltol.** MS (ESI), (*m/z*) calc. for $C_6H_6O_3$ = 126.03, found: 125.4 $[M-H]^+$.

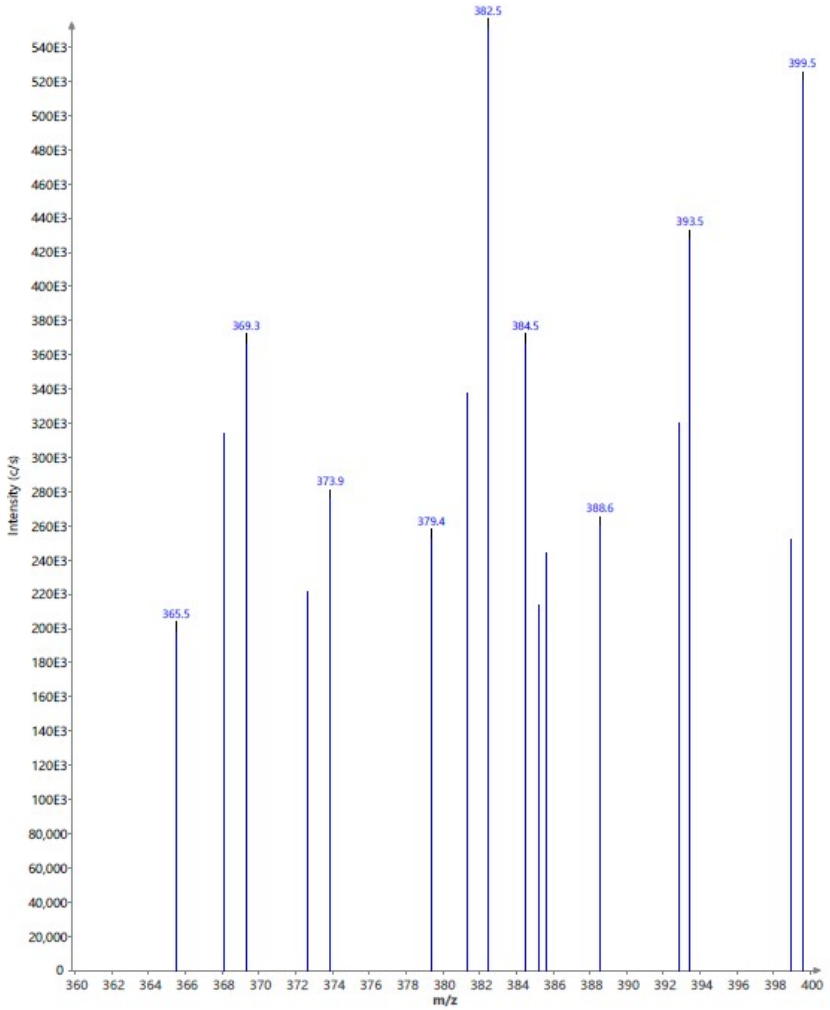

Fig. S3. ESI–MS of **$[MoO_2(Mal)_2]$**. MS (ESI), (*m/z*) calc. for $C_{12}H_{10}MoO_8$ = 378.14, found: 379.4. $[M+H]^+$.

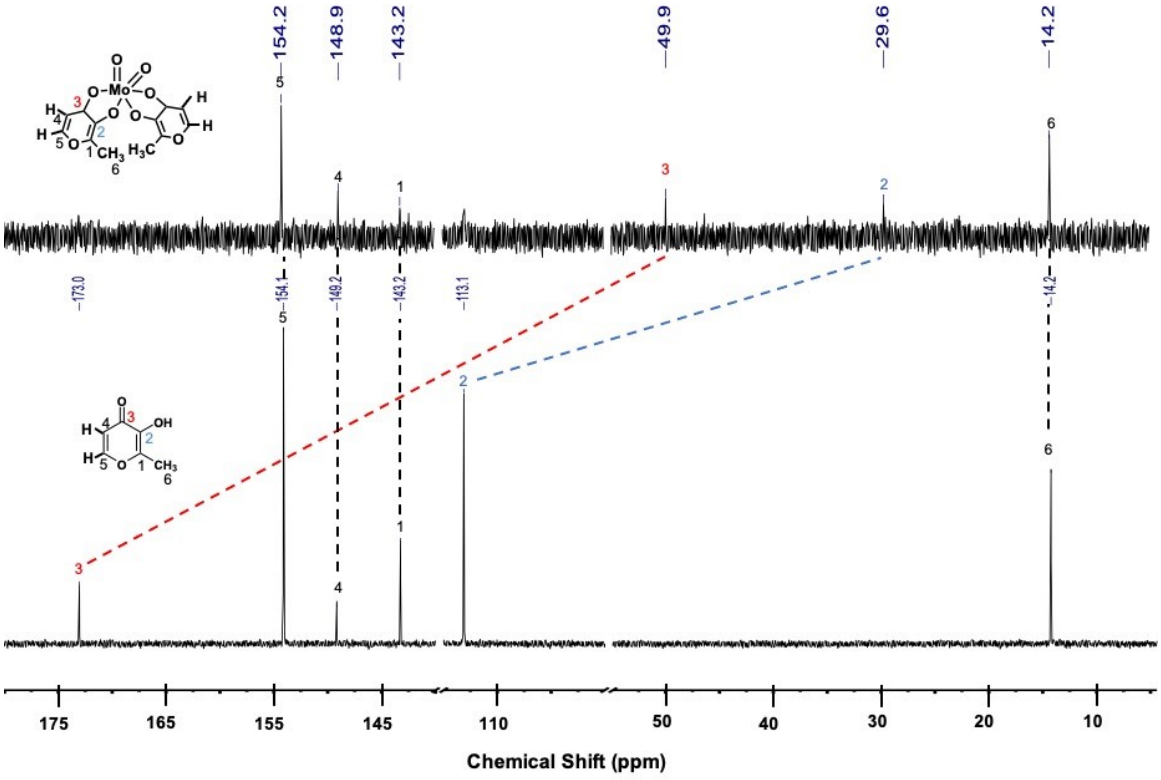

Fig. S4. Stacked ^{13}C NMR spectra of **Maltol** and **[MoO_2(Mal)$_2$]**. ^{13}C NMR were recorded at 25 °C in $CDCl_3$ solvent.

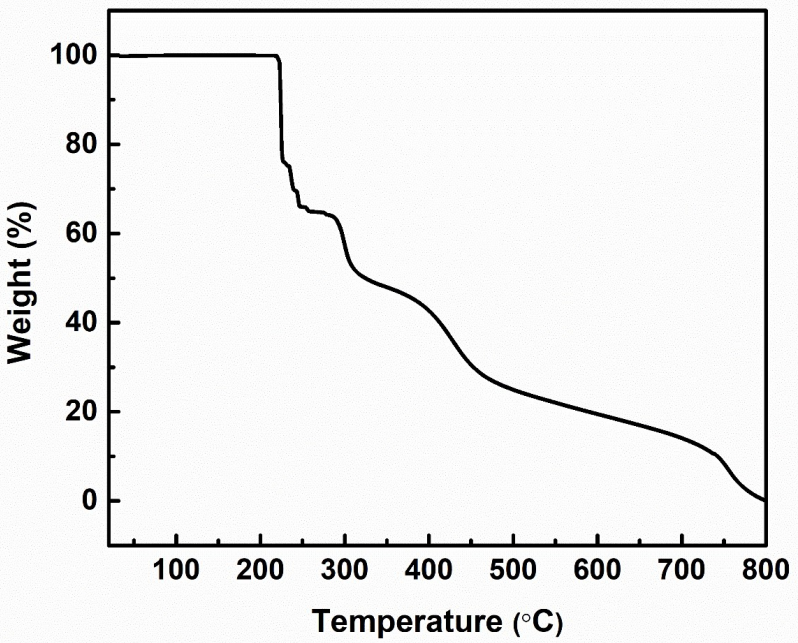

Fig. S5. Thermogravimetric analysis (TGA) of **[MoO_2(Mal)$_2$]**. Initial weight of the compound **1** (7.43 g) was subjected to thermal analysis at a heating rate of 20 °C min^{-1} under an argon atmosphere.

Table S1. Crystallographic data and structure refinement for **Maltol** complex.

Empirical formula	$C_{30}H_{30}O_{15}$
M	630.54
Cryst sym	Triclinic
space group	P-1
a (Å)	6.9493(4)
b (Å)	7.1414(4)
c (Å)	30.2196(13)
α (deg)	85.419(4)
β (deg)	86.684(4)
γ (deg)	70.931(5)
V (Å^3)	1412.09(13)
Z	2
D_{calc} (g cm^{-3})	1.483
μ (Mo Kα) (mm^{-1})	1.031
F (000)	660.0
Range for data collection (deg)	5.872 to 147.79
Data/ Parameters	5419/0/416
Temp (K)	150
reflns collected	18978
R^a [I > 2σ(I)]	R_1= 0.0907, wR_2 = 0.2389
$R_w{}^b$ [all data]	R_1= 0.1352, wR_2 = 0.3199
S [goodness of fit]	1.081
max/ min res (e Å^{-3})	0.72/ -0.91

The CIF file can be obtained from CCDC. CCDC id: 2292692. Database identifier: JISLEG

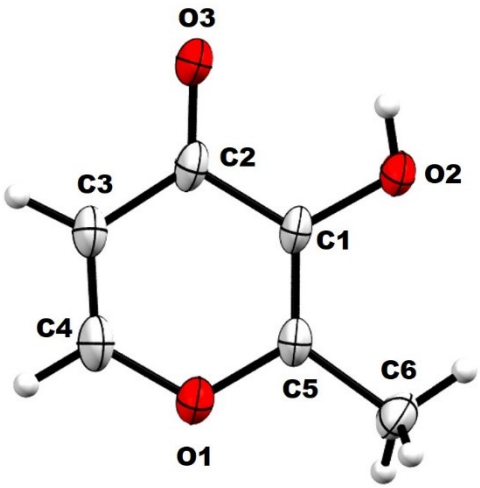

Fig. S6. ORTEP diagram of **Maltol** in 50% occupancy.

Table S2. Bond lengths for **Maltol**.

Atom	Atom	Length/Å
O1	C4	1.353(4)
O1	C5	1.360(4)
O2	H2	0.84
O2	C1	1.366(4)
O3	C2	1.247(5)
O4	C10	1.339(5)
O4	C11	1.363(5)
O5	H5	0.84
O5	C7	1.358(4)
O6	C8	1.237(5)
O7	C14	1.366(4)
O7	C15	1.350(5)
O8	H8	0.84
O8	C13	1.354(4)
O9	C17	1.234(4)
O10	C22	1.348(5)
O10	C23	1.367(5)
O11	H11	0.84
O11	C19	1.362(5)
O12	C20	1.238(5)
O13	C26	1.362(4)
O13	C27	1.342(5)
O14	H14	0.84
O14	C25	1.359(4)
O15	C29	1.234(4)
C1	C2	1.446(5)
C1	C5	1.340(5)
C2	C3	1.425(5)
C3	H3	0.95
C3	C4	1.334(6)
C4	H4	0.95
C5	C6	1.489(5)
C6	H6A	0.98
C6	H6B	0.98
C6	H6C	0.98
C7	C8	1.443(5)
C7	C11	1.344(5)
C8	C9	1.451(5)
C9	H9	0.95
C9	C10	1.341(6)
C10	H10	0.95

C11	C12	1.493(5)
C12	H12A	0.98
C12	H12B	0.98
C12	H12C	0.98
C13	C14	1.352(5)
C13	C17	1.434(5)
C14	C18	1.473(5)
C15	H15	0.95
C15	C16	1.323(5)
C16	H16	0.95
C16	C17	1.444(5)
C18	H18A	0.98
C18	H18B	0.98
C18	H18C	0.98
C19	C20	1.451(5)
C19	C23	1.335(6)
C20	C21	1.432(5)
C21	H21	0.95
C21	C22	1.335(6)
C22	H22	0.95
C23	C24	1.495(5)
C24	H24A	0.98
C24	H24B	0.98
C24	H24C	0.98
C25	C26	1.348(5)
C25	C29	1.447(5)
C26	C30	1.481(6)
C27	H27	0.95
C27	C28	1.326(5)
C28	H28	0.95
C28	C29	1.448(5)
C30	H30A	0.98
C30	H30B	0.98
C30	H30C	0.98

Table S3. Bond angles for **Maltol**.

Atom	Atom	Atom	Angle/˚
C4	O1	C5	118.9(3)
C1	O2	H2	109.5
C10	O4	C11	119.4(3)
C7	O5	H5	109.5
C15	O7	C14	119.1(3)
C13	O8	H8	109.5
C22	O10	C23	119.0(3)
C19	O11	H11	109.5
C27	O13	C26	119.3(3)
C25	O14	H14	109.5
O2	C1	C2	118.7(3)
C5	C1	O2	119.9(3)
C5	C1	C2	121.4(3)
O3	C2	C1	120.8(3)
O3	C2	C3	124.5(3)
C3	C2	C1	114.7(3)
C2	C3	H3	119.8
C4	C3	C2	120.4(3)
C4	C3	H3	119.8
O1	C4	H4	118.3
C3	C4	O1	123.4(4)
C3	C4	H4	118.3
O1	C5	C6	112.7(3)
C1	C5	O1	121.2(3)
C1	C5	C6	126.0(3)
C5	C6	H6A	109.5
C5	C6	H6B	109.5
C5	C6	H6C	109.5
H6A	C6	H6B	109.5
H6A	C6	H6C	109.5
H6B	C6	H6C	109.5
O5	C7	C8	118.1(3)
C11	C7	O5	119.7(3)
C11	C7	C8	122.2(4)
O6	C8	C7	122.2(4)
O6	C8	C9	123.8(3)
C7	C8	C9	114.0(3)
C8	C9	H9	120.1
C10	C9	C8	119.8(3)
C10	C9	H9	120.1
O4	C10	C9	123.9(4)

O4	C10	H10	118.1
C9	C10	H10	118.1
O4	C11	C12	112.8(3)
C7	C11	O4	120.7(3)
C7	C11	C12	126.4(4)
C11	C12	H12A	109.5
C11	C12	H12B	109.5
C11	C12	H12C	109.5
H12A	C12	H12B	109.5
H12A	C12	H12C	109.5
H12B	C12	H12C	109.5
O8	C13	C17	118.7(3)
C14	C13	O8	119.2(3)
C14	C13	C17	122.0(3)
O7	C14	C18	112.6(3)
C13	C14	O7	120.4(3)
C13	C14	C18	126.9(3)
O7	C15	H15	118.1
C16	C15	O7	123.7(3)
C16	C15	H15	118.1
C15	C16	H16	119.8
C15	C16	C17	120.3(4)
C17	C16	H16	119.8
O9	C17	C13	121.6(3)
O9	C17	C16	124.1(4)
C13	C17	C16	114.3(3)
C14	C18	H18A	109.5
C14	C18	H18B	109.5
C14	C18	H18C	109.5
H18A	C18	H18B	109.5
H18A	C18	H18C	109.5
H18B	C18	H18C	109.5
O11	C19	C20	118.3(3)
C23	C19	O11	119.7(3)
C23	C19	C20	122.0(4)
O12	C20	C19	121.6(4)
O12	C20	C21	124.1(3)
C21	C20	C19	114.2(3)
C20	C21	H21	119.9
C22	C21	C20	120.2(3)
C22	C21	H21	119.9
O10	C22	H22	118.2
C21	C22	O10	123.7(4)

C21	C22	H22	118.2
O10	C23	C24	112.1(3)
C19	C23	O10	120.8(3)
C19	C23	C24	127.1(4)
C23	C24	H24A	109.5
C23	C24	H24B	109.5
C23	C24	H24C	109.5
H24A	C24	H24B	109.5
H24A	C24	H24C	109.5
H24B	C24	H24C	109.5
O14	C25	C29	118.1(3)
C26	C25	O14	119.9(3)
C26	C25	C29	122.0(3)
O13	C26	C30	113.2(3)
C25	C26	O13	120.7(4)
C25	C26	C30	126.1(3)
O13	C27	H27	118
C28	C27	O13	124.0(4)
C28	C27	H27	118
C27	C28	H28	119.9
C27	C28	C29	120.2(4)
C29	C28	H28	119.9
O15	C29	C25	121.8(3)
O15	C29	C28	124.4(3)
C25	C29	C28	113.8(3)
C26	C30	H30A	109.5
C26	C30	H30B	109.5
C26	C30	H30C	109.5
H30A	C30	H30B	109.5
H30A	C30	H30C	109.5
H30B	C30	H30C	109.5

Table S4. Crystallographic data and structure refinement for complex **1 [$MoO_2(Mal)_2$]**.

Empirical formula	$C_{12}H_{10}MoO_8$
M	378.14
Cryst sym	monoclinic
space group	C2/c
a (Å)	10.0766(11)
b (Å)	10.5933(12)
c (Å)	12.4062(12)
α (deg)	90
β (deg)	93.045
γ (deg)	90
V ($Å^3$)	1322.4(2)
Z	4
D_{calc} (g cm^{-3})	1.899
μ (Mo Kα) (mm^{-1})	1.030
F (000)	752.0
Range for data collection (deg)	5.584 to 49.994
Data/ Parameters	1153/0/97
Temp (K)	150
reflns collected	11928
R^a [I > 2σ(I)]	R_1= 0.0171, wR_2 = 0.0458
R_w^b [all data]	R_1= 0.0176, wR_2 = 0.0461
S [goodness of fit]	1.151
max/ min res (e $Å^{-3}$)	0.27/-0.25

The CIF file can be obtained from CCDCD. CCDC id: 2292693. Database identifier: JISLIK

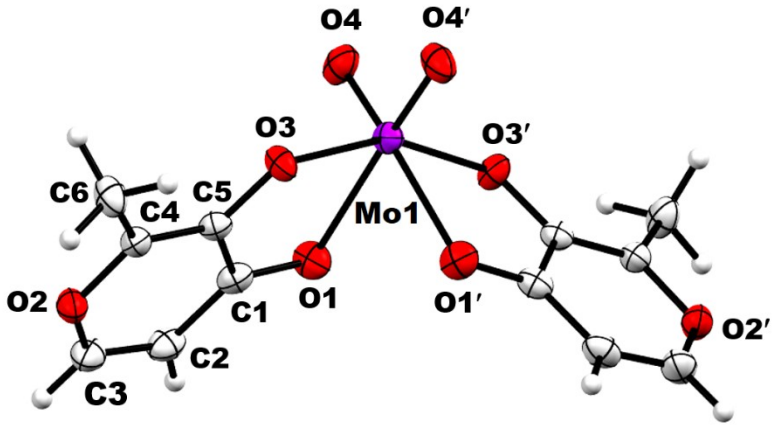

Fig. S7. ORTEP diagram of Complex **1 [$MoO_2(Mal)_2$]** with 50% occupancy.

Table S5. Bond lengths for complex **1 [$MoO_2(Mal)_2$]**.

Atom	Atom	Length/Å
Mo1	O1	2.2396(15)
Mo1	$O1^1$	2.2396(14)
Mo1	O3	1.9951(13)
Mo1	$O3^1$	1.9952(13)
Mo1	$O4^1$	1.7016(14)
Mo1	O4	1.7016(14)
O1	C1	1.264(3)
O2	C3	1.351(2)
O2	C4	1.361(2)
O3	C5	1.342(2)
C1	C2	1.423(3)
C1	C5	1.437(3)
C2	C3	1.341(3)
C4	C5	1.354(3)
C4	C6	1.486(3)

Table S6. Bond angles for complex **1 [$MoO_2(Mal)_2$]**.

Atom	Atom	Atom	Angle/˚
$O1^1$	Mo1	O1	79.54(8)
O3	Mo1	O1	75.31(5)
$O3^1$	Mo1	O1	86.04(5)
O3	Mo1	$O1^1$	86.04(5)
$O3^1$	Mo1	$O1^1$	75.31(5)
O3	Mo1	$O3^1$	155.77(8)
O4	Mo1	$O1^1$	163.02(6)
$O4^1$	Mo1	$O1^1$	89.07(7)
O4	Mo1	O1	89.08(7)
$O4^1$	Mo1	O1	163.02(6)
$O4^1$	Mo1	$O3^1$	103.34(6)
O4	Mo1	$O3^1$	91.49(6)
$O4^1$	Mo1	O3	91.50(6)
O4	Mo1	O3	103.34(6)
O4	Mo1	$O4^1$	104.58(11)
C1	O1	Mo1	112.61(12)
C3	O2	C4	120.19(16)
C5	O3	Mo1	118.46(11)
O1	C1	C2	126.69(18)
O1	C1	C5	116.74(17)
C2	C1	C5	116.57(18)

C3	C2	C1	118.77(19)
C2	C3	O2	123.49(19)
O2	C4	C6	114.11(16)
C5	C4	O2	119.85(17)
C5	C4	C6	126.03(18)
O3	C5	C1	115.94(16)
O3	C5	C4	122.95(17)
C4	C5	C1	121.08(18)

4. $[MoO_2(Mal)_2]$ catalyzed oxidation reactions

Table S7. $[MoO_2(Mal)_2]$ catalyzed oxidation reactions.

Entry	**Substrate**[a]	**Catalyst mol %**	**H_2O_2 (mmol)**	***t*-BuOOH (TBHP) (mmol)**	**% Conversion (GC)**	**Temperature (°C)**	**Time (h)**
1	Diphenylmethane	5	60	-	64.46	80 °C	12
2	Toluene	1	60	-	No	80°C	24
3		3	60	-	No	80°C	24
4		5	60	-	No	80 °C	24
5		5	-	1	18.58	80 °C	18
6		5 *Reused *Reused	- - -	2 2 2	64.57 *Conversion was monitored by TLC	80 °C	12
7		5	-	5	84.42	80 °C	18
8		5	-	5	99.66	80 °C	24
9	Styrene[b]	0.25	-	2.5	54.36	100 °C	6
10	Hypoxanthine	5	-	-	No	RT	20
11	Hypoxanthine	5		1	40.11	RT	15
12	Hypoxanthine	5		1	37.42	80 °C	15

[a] 1 mmol substrate was taken in acetonitrile for the reaction in inert condition. [b]Reaction was performed in a solvent-free condition and 2.5 mmol of substrate was taken.

GC method for analysis of catalysis reactions of diphenylmethane, toluene, and styrene. Celite filtration under vacuum was performed prior to the GC analysis. Gas chromatography analysis was carried out using Agilent Technologies 7890 B network GC System, equipped with an Agilent Technologies G4513A series auto sampler and a glass capillary HP-5, ID: 0.32 mm, length: 30 m, film thickness: 0.25 µm; packed with non-polar polymer [(5%-phenyl)-methylpolysiloxane. A helium carrier gas flow 1.0 ml/min; injection temperature 280°C oven temperature program 50°C for 5min, @ 10°C/min to 180°C, post run: 280°C held for 2 min (total run time: 18 min); Splitless injection at a volume of 1 µl by auto sampler.

A) Oxidation of diphenylmethane.

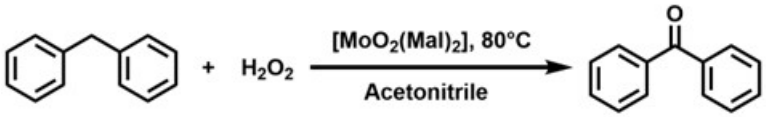

To a 100 mL two neck round bottom flask fitted with a reflux condenser and a magnetic stirrer bar in which diphenylmethane (168 mg, 1 mmol), **$[MoO_2(Mal)_2]$** (5 mol%) and acetonitrile (1 mL) was added. Then H_2O_2 (1.40 mL, 60 mmol) was added dropwise over a period of 5 minutes. The reaction mixture was stirred at 80°C for 12 hours. Reaction was quenched, filtered through celite under vacuum prior to GC analysis.

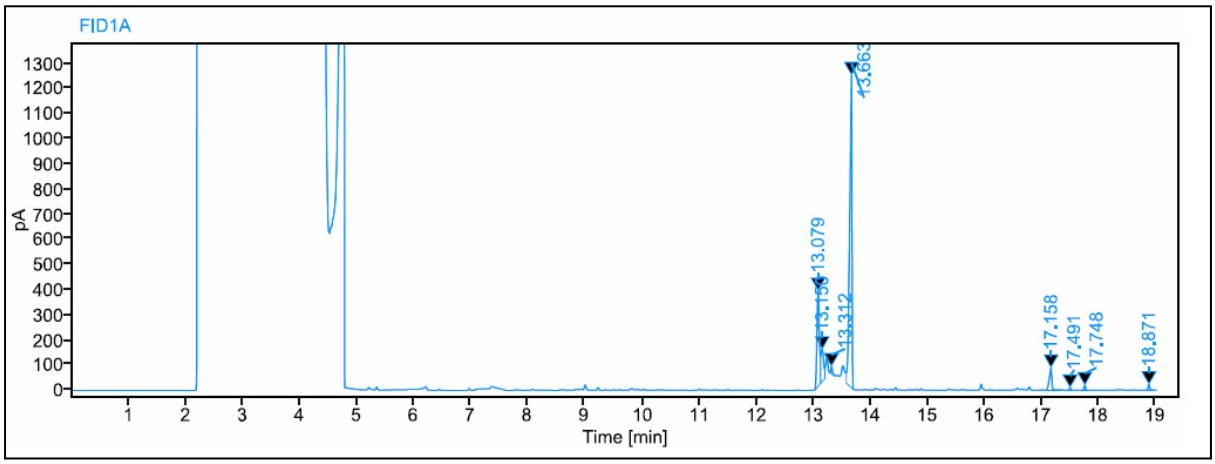

Fig. S8. GC chromatogram of oxidation of diphenylmethane catalyzed by **$[MoO_2(Mal)_2]$** by using 60 mmol H_2O_2 as an oxidant. % Conversion = 64.46.

B) Oxidation of toluene.

(a)

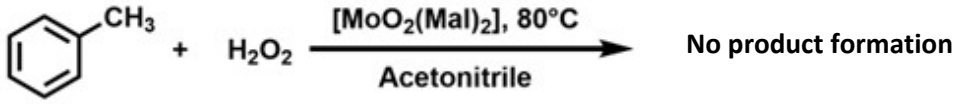

(b)

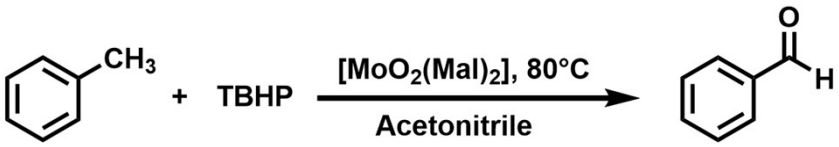

a) To a 100 mL two neck round bottom flask fitted with a reflux condenser and a magnetic stirrer bar in which toluene (0.1mL, 1 mmol), **[$MoO_2(Mal)_2$]** (5 mol%) and acetonitrile (1 mL) was added. Then H_2O_2 (1.40 mL, 60 mmol) was added dropwise over a period of 5 minutes. The reaction mixture was stirred at 80°C for 12 hours. No progress in the reaction was observed.

b) To a 100 mL two neck round bottom flask fitted with a reflux condenser and a magnetic stirrer bar in which toluene (0.1mL, 1 mmol), **[$MoO_2(Mal)_2$]** (5 mol%) and acetonitrile (1 mL) was added. Then TBHP in 5-6 M decane (1, 2, and 5 mmol, respectively) was added dropwise. The reaction mixture was then stirred at 80 °C for 12 – 24 h. Reaction was quenched, filtered through celite under vacuum prior to GC analysis.

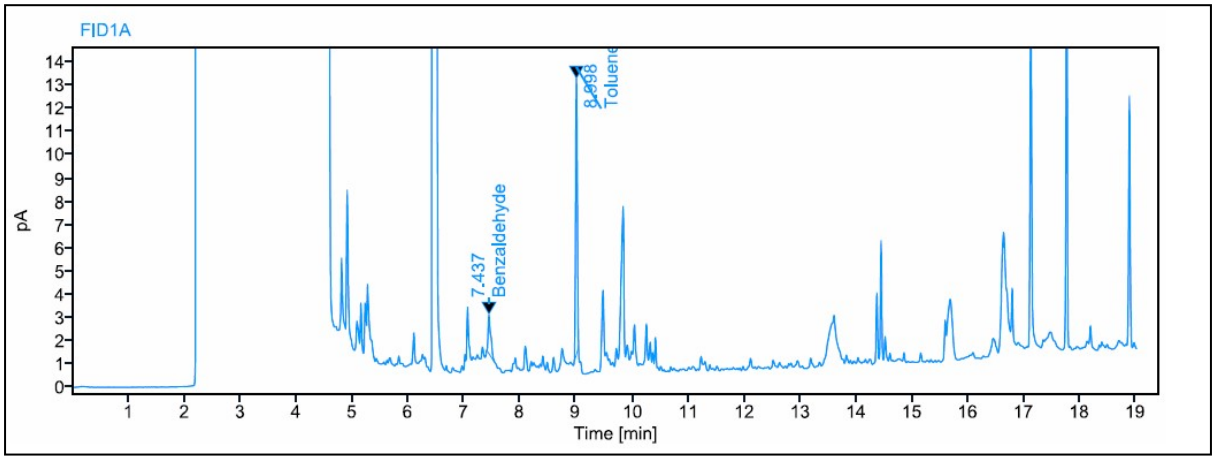

Fig. S9. GC chromatogram of oxidation of toluene to benzaldehyde catalyzed by **[$MoO_2(Mal)_2$]** by using 1 mmol TBHP as an oxidant for reaction carried out for 12 h at 80 °C. % Conversion = 18.58.

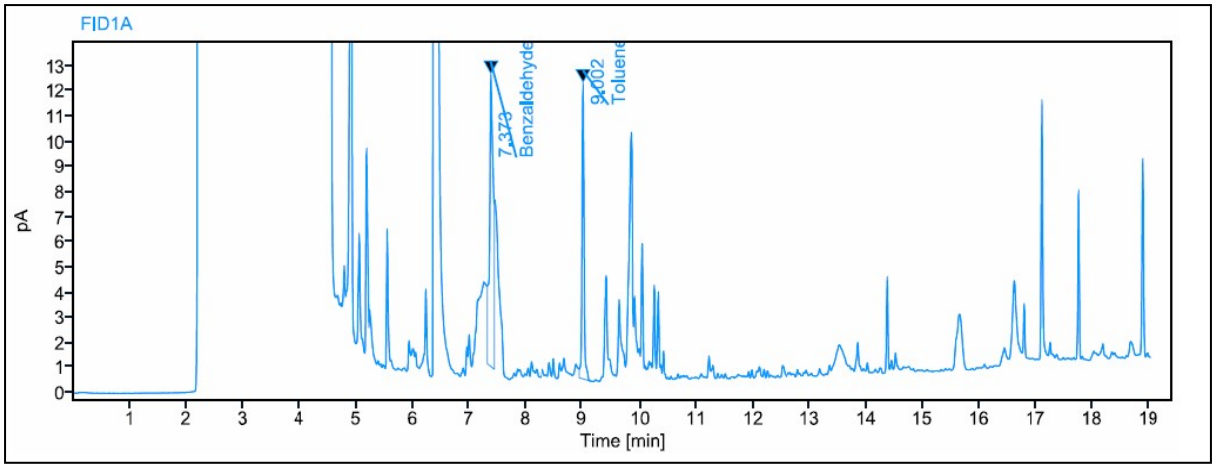

Fig. S10. Oxidation of toluene to benzaldehyde catalyzed by **[$MoO_2(Mal)_2$]** by using 2 mmol TBHP as an oxidant for reaction carried out for 12 h at 80 °C. % Conversion = 64.57.

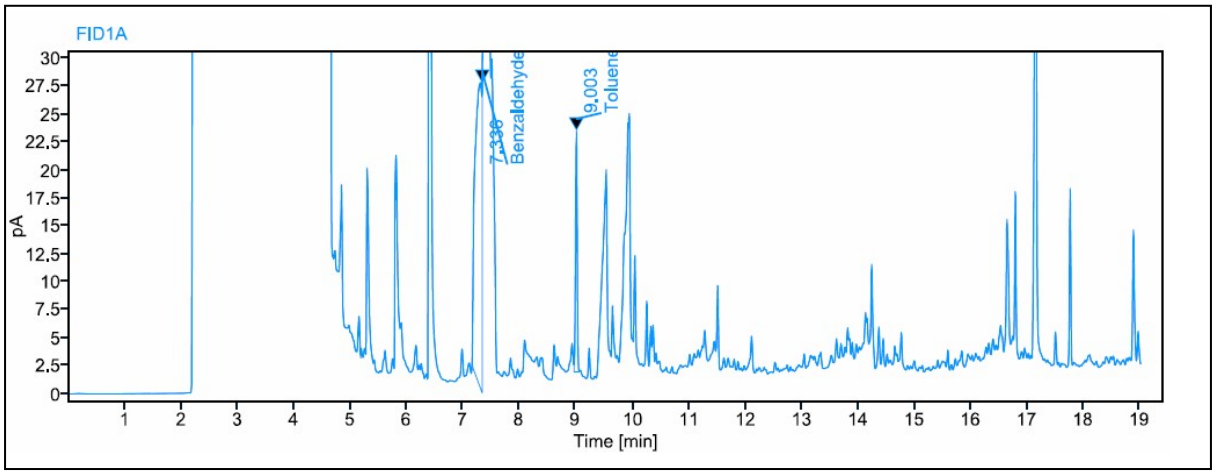

Fig. S11. GC chromatogram of oxidation of toluene to benzaldehyde catalyzed by **[$MoO_2(Mal)_2$]** by using 5 mmol TBHP as an oxidant for reaction carried out for 18 h at 80 °C. % Conversion = 84.42.

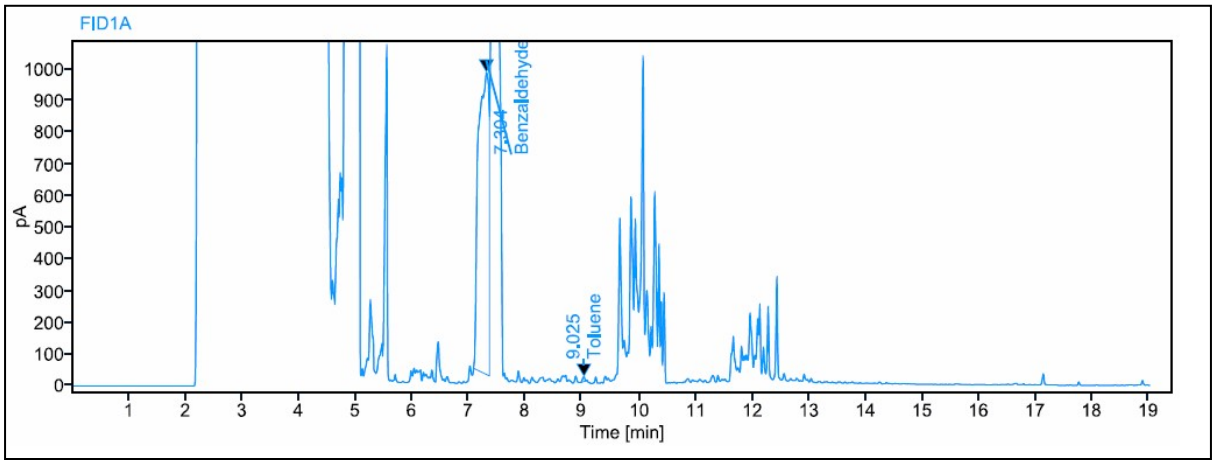

Fig. S12. GC chromatogram of oxidation of toluene to benzaldehyde catalyzed by **[$MoO_2(Mal)_2$]** by using 5 mmol TBHP as an oxidant for reaction carried out for 24 h at 80 °C. % Conversion = 99.66**.**

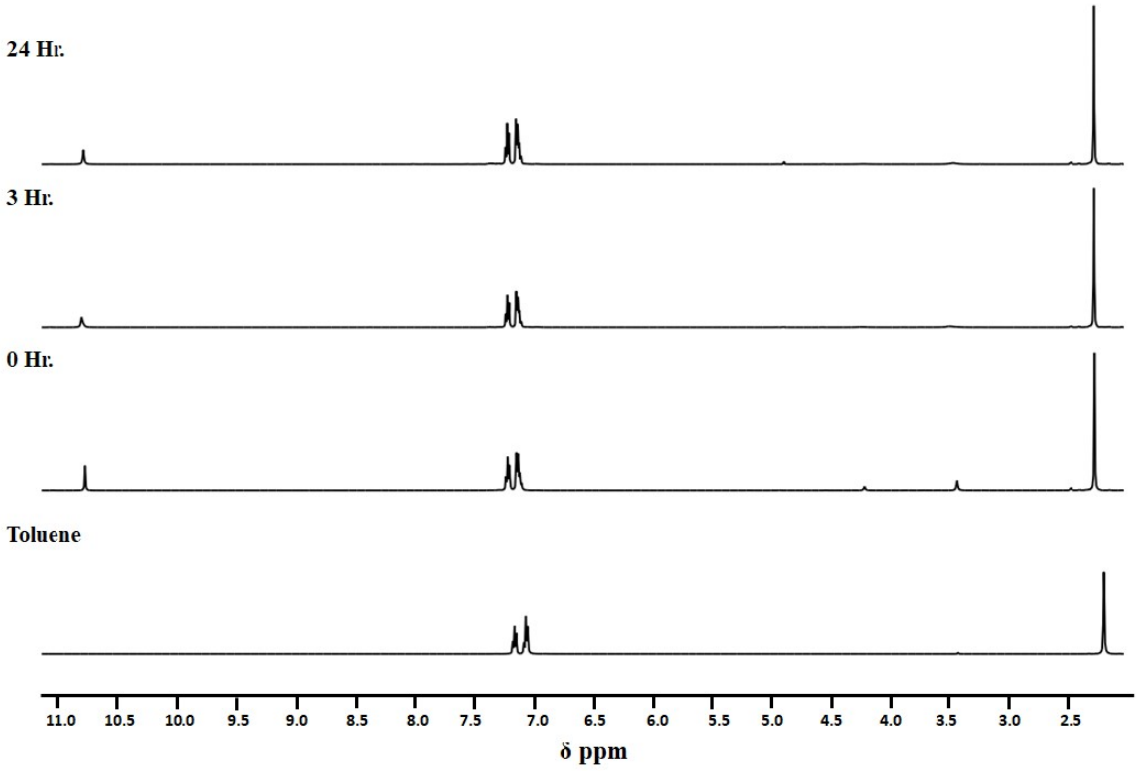

Fig. S13. Stacked ^{1}H NMR spectra of pure toluene (bottom) and its oxidation reaction mixtures catalysed by **[$MoO_2(Mal)_2$]** at different time intervals in *dmso-d_6*. The reaction was performed at room temperature without the presence acetonitrile solvent with 5 mol% catalyst and 5 mmol TBHP under N_2 atmosphere.

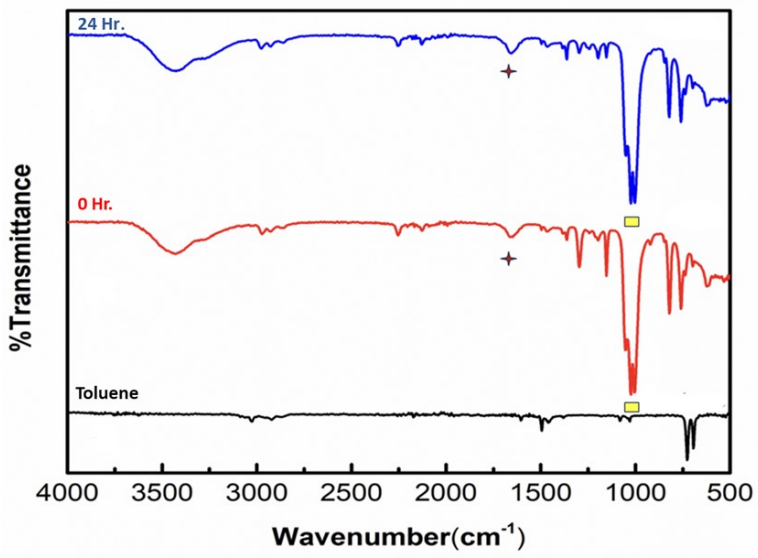

Fig. S14. Stacked ATR-FTIR spectra of toluene and its oxidation reaction mixtures at 0, and 24 h respectively. The reaction was performed at room temperature without the presence acetonitrile solvent with 5 mol% catalyst and 5 mmol TBHP. The absorption band at 1656 cm^{-1} corresponds to -C=O stretching in benzaldehyde (red star) appeared in the FTIR spectra of the reaction mixture.

C) Epoxidation of styrene.

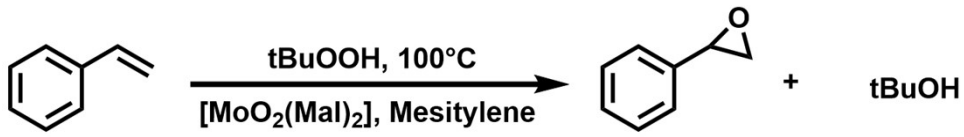

To a 100 mL two neck round bottom flask fitted with a reflux condenser and a magnetic stirrer bar in which **[$MoO_2(Mal)_2$]** (2.38 mg, 0.25 mol%) was added based on styrene. To this TBHP in 5-6 M decane (0.5 mL, 2.5 mmol) was added dropwise over a period of 2 min. Then styrene (0.286 mL, 2.50 mmol) was added with continuous stirring over a period of 20 min and then mesitylene (0.0486 mL, 0.349 mmol) was added as an internal standard. The reaction mixture was stirred at 100 °C for 6 hours. Reaction was quenched, filtered through celite under vacuum prior to GC analysis.

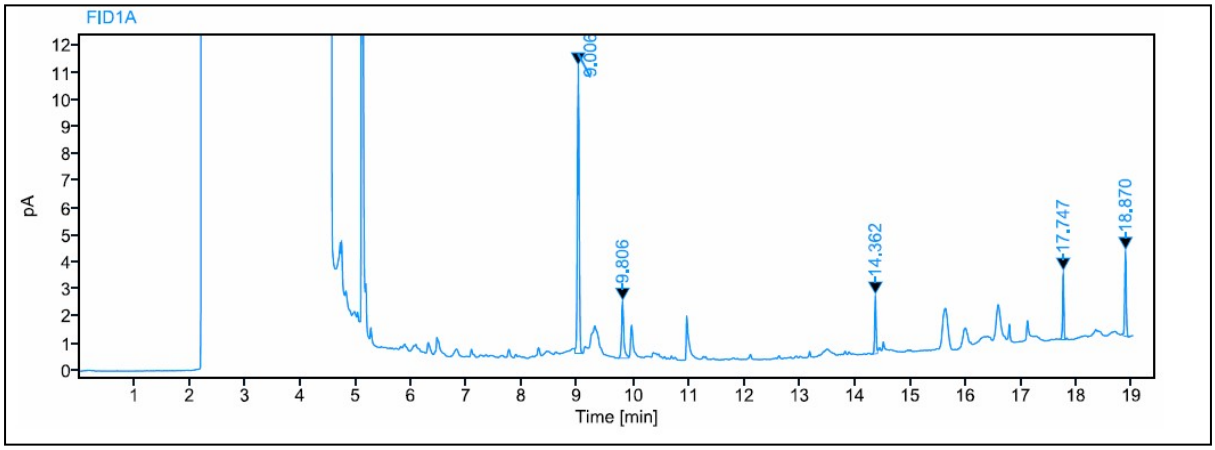

Fig. S15. GC chromatogram of oxidation of styrene to styrene oxide catalyzed by **[$MoO_2(Mal)_2$]** complex using 2.5 mmol TBHP as an oxidant. % Conversion =54.36.

D) Oxidation of hypoxanthine

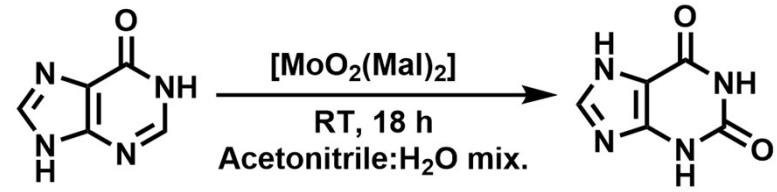

Hypoxanthine **Xanthine**

To a 100 mL two neck round bottom flask fitted with a reflux condenser and a magnetic stirrer bar in which hypoxanthine (0.136 gm, 1 mmol), **[MoO_2(Mal)$_2$]** (5 mol%), acetonitrile (1 mL) and water (1 mL) was added. Then TBHP in 5-6 M decane (1 mmol) was added dropwise. The reaction mixture was stirred at room temperature for 18 hours. Reaction was quenched, filtered through celite under vacuum prior to GC analysis.

GC method for analysis of catalysis reaction of Hypoxanthine to Xanthine:

Gas chromatography analysis was carried out using Agilent Technologies 7890 B network GC system, equipped with an Agilent Technologies G4513A series auto sampler and a glass capillary HP-5, ID: 0.32 mm, length: 30 m, film thickness:0.25 µm; packed with non-polar polymer [(5%-phenyl)-methylpolysiloxane. A helium carrier gas flow 0.5 ml/min; injection temperature 280°C oven temperature program 120°C for 1 min, @ 15°C/min to 195°C, 5°C/min to 260°C, post run: 280°C held for 2 min (total run time: 18 min); Splitless injection at a volume of 1 µl by auto sampler.

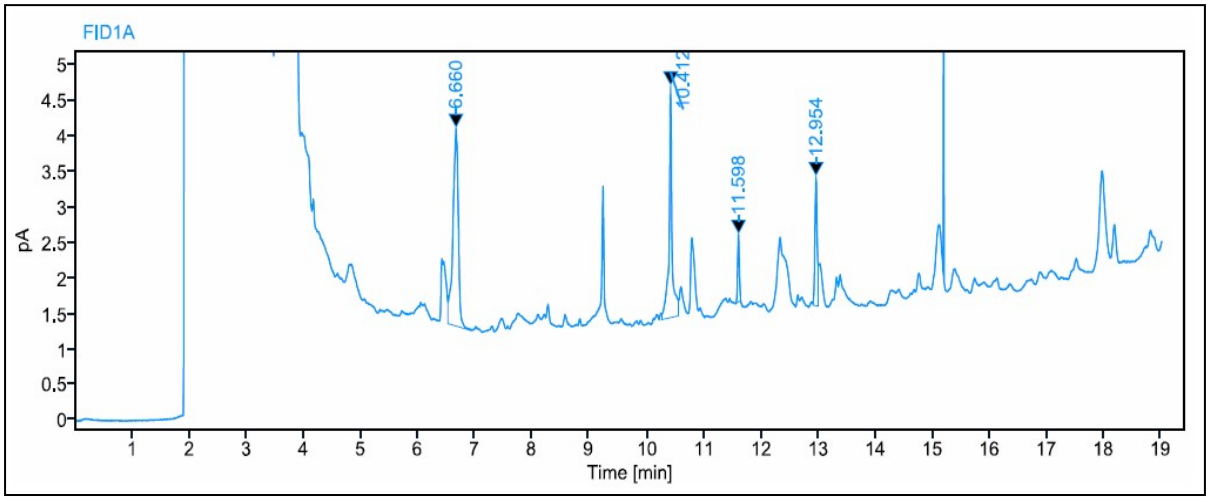

Fig. S16. GC chromatogram of oxidation of hypoxanthine to xanthine catalysed by **[MoO_2(Mal)$_2$]** by using 1 mmol TBHP as an oxidant at room temperature for 15 h. % Conversion = 40.11.

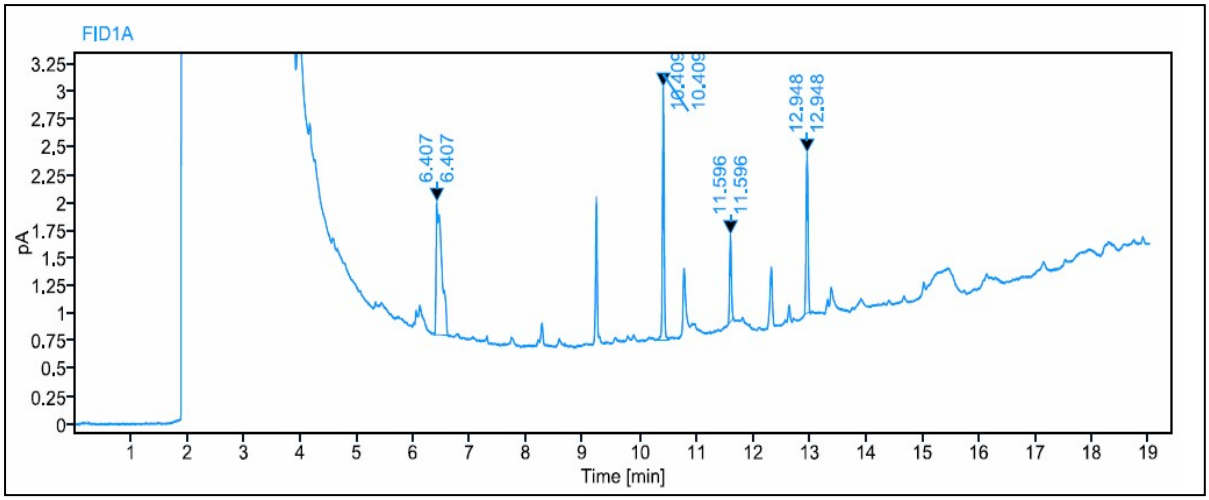

Fig. S17. GC chromatogram of oxidation of hypoxanthine to xanthine catalyzed by **[$MoO_2(Mal)_2$]** by using 1 mmol TBHP as an oxidant at 80°C for 15 h. % Conversion = 37.42.

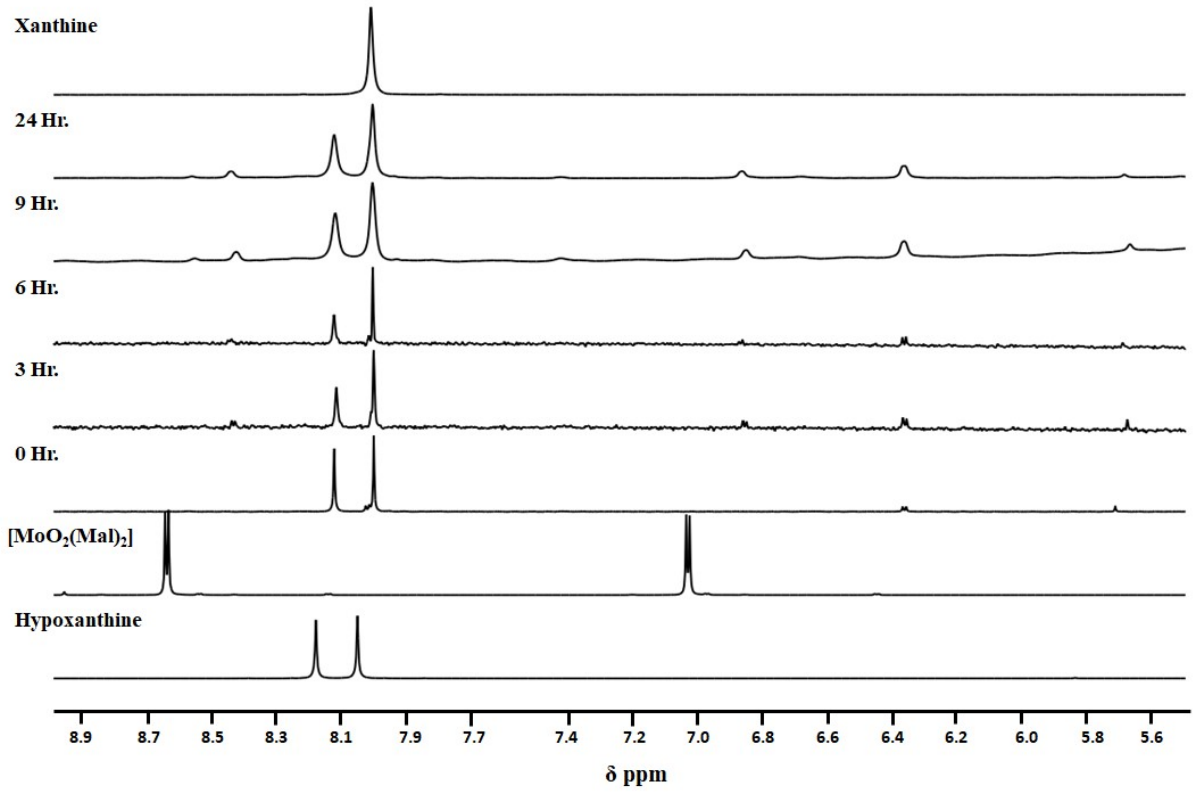

Fig. S18. Stacked ^{1}H NMR spectra of (top to bottom) xanthine, reaction mixture after 24, 9, 6, 3, 0 h, **[$MoO_2(Mal)_2$]** and hypoxanthine in *dmso-d_6* respectively. The reaction was performed at room temperature in the presence DMSO solvent with 5 mol% catalyst and 1 mmol TBHP.

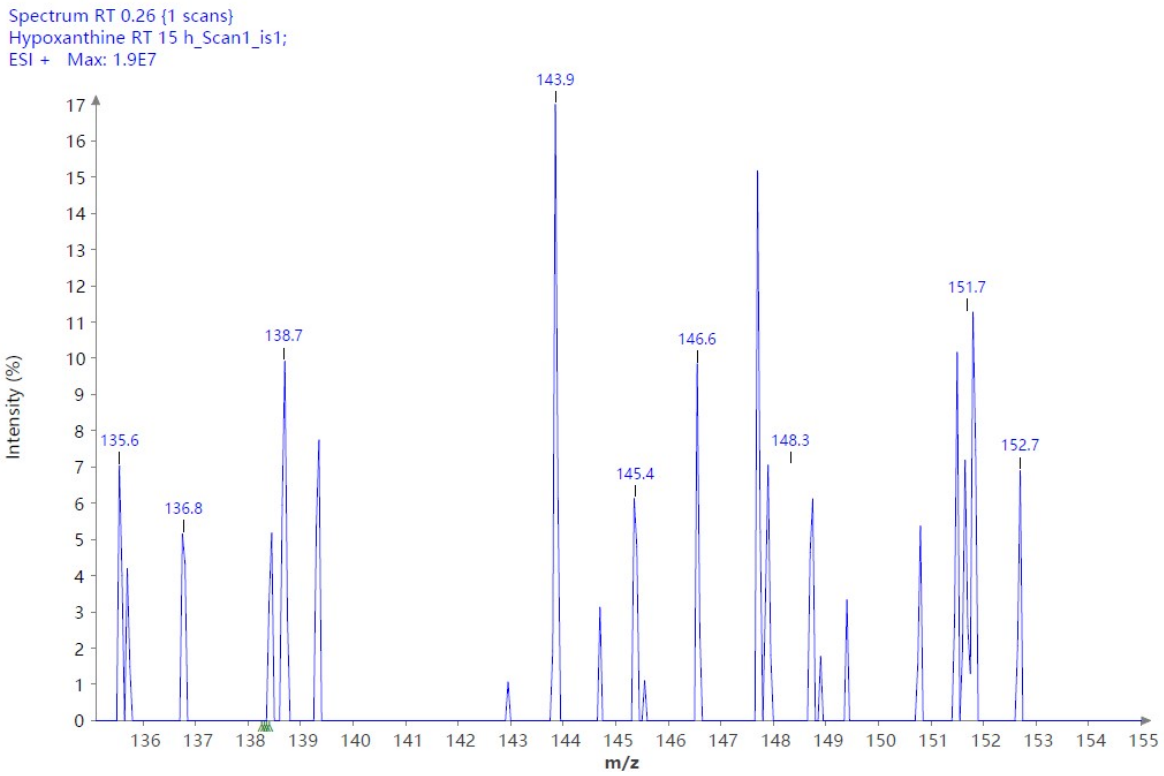

Fig. S19. TLC ESI–MS of the reaction mixture of hypoxanthine oxidation reaction catalysed by **[MoO_2(Mal)$_2$].** (*m/z*) calc. for $C_5H_4N_4O_2$ = 152.11, found: 152.7 $[M]^+$.

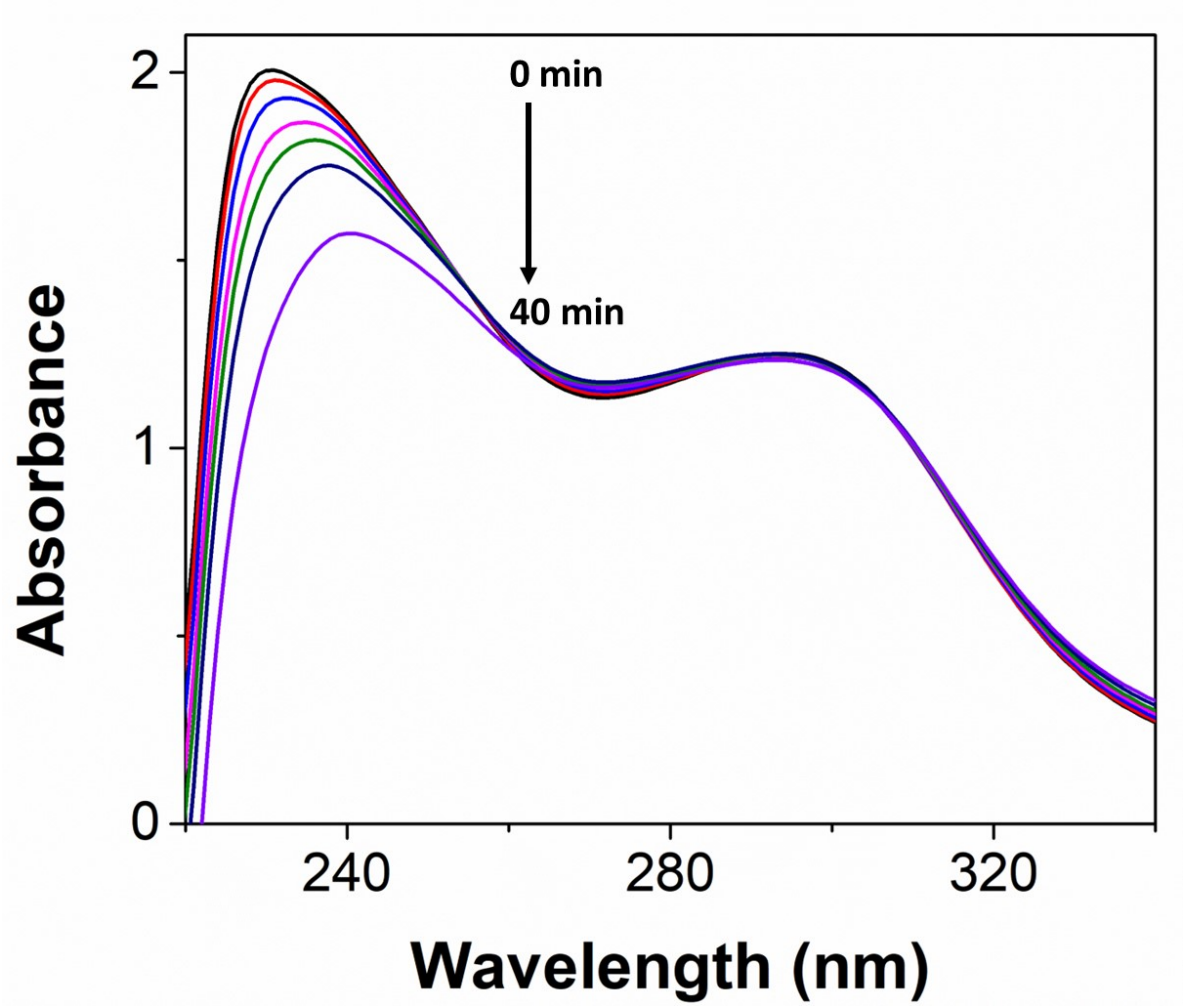

Fig. S20. Absorption spectra of **[$MoO_2(Mal)_2$]** in the presence of NBT and TBHP in acetonitrile solvent at 25 °C at different time intervals showing reducing absorption intensity of NBT at λ_{max} = 230 nm over the period of 40 min. Concentrations [NBT] = 19 × 10^{-6} M, **[$MoO_2(Mal)_2$]** = 1.25 × 10^{-5} M, [TBHP] = 13.75 × 10^{-5} M in ACN at 25 °C.

5. Control Studies

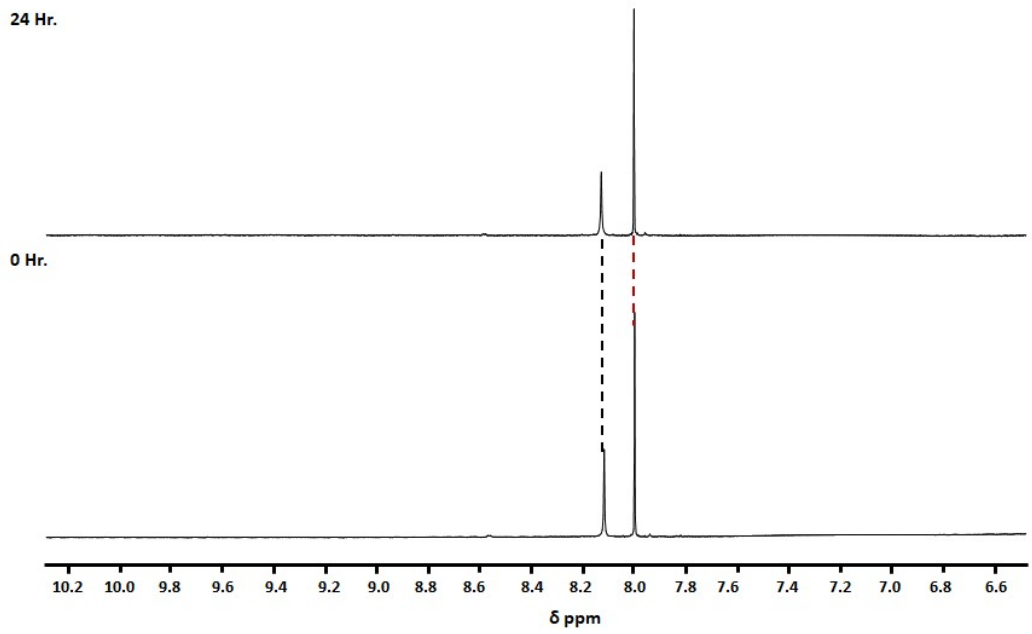

Fig. S21. Stacked ^{1}H NMR spectra of the reaction mixture of hypoxanthine oxidation reaction in the presence of **$(NH_4)_6Mo_7O_{24}.4H_2O$** catalyst at 0 hr (bottom) and 24 hr (top) in *dmso-d_6*. The reaction was performed at room temperature in the presence DMSO solvent with 5 mol% catalyst and 1 mmol TBHP.

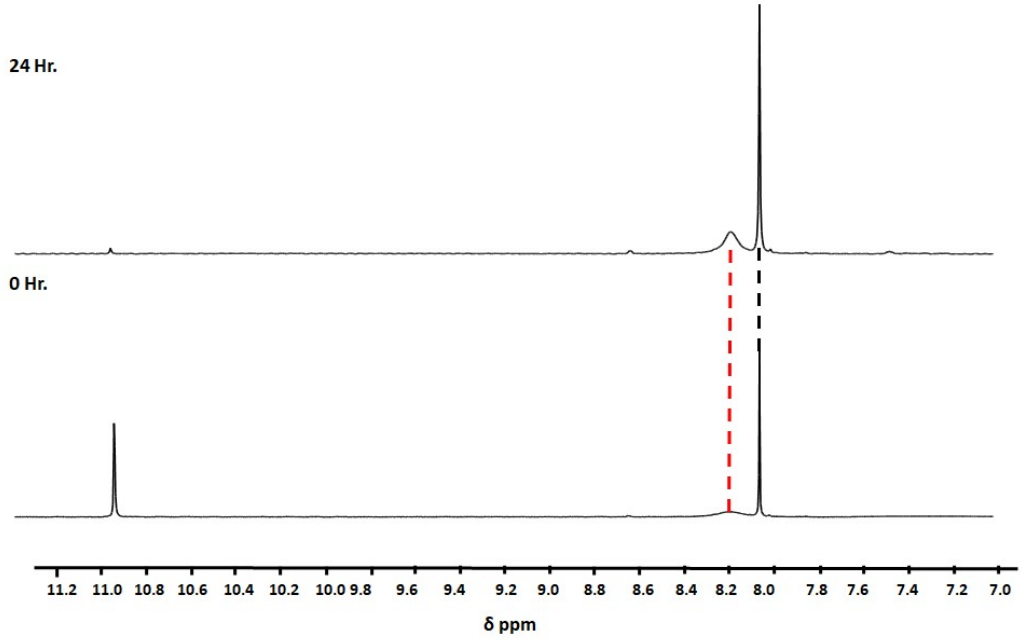

Fig. S22. Stacked ^{1}H NMR spectra of the reaction mixture of hypoxanthine oxidation reaction in the presence of **$C_{10}H_{14}MoO_6$** [$MoO_2(acac)_2$] catalyst at 0 hr (bottom) and 24 hr (top) in *dmso-d_6*. The reaction was performed at room temperature in the presence DMSO solvent with 5 mol% catalyst and 1 mmol TBHP.

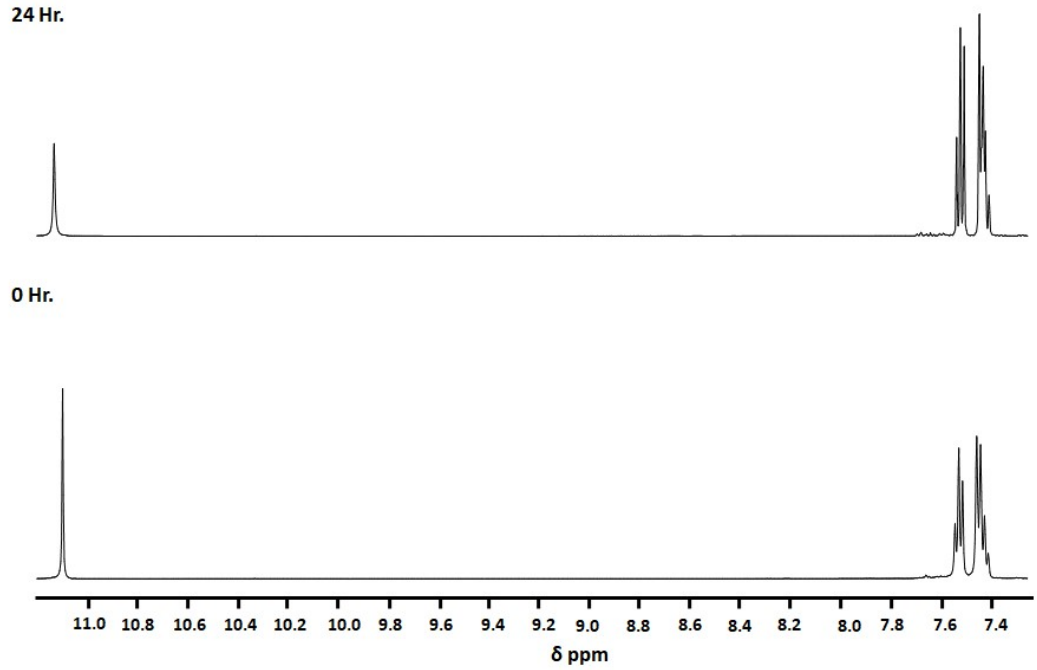

Fig. S23. Stacked ^{1}H NMR spectra of the reaction mixture of toluene oxidation reaction in the presence of **$(NH_4)_6Mo_7O_{24}$**. $4H_2O$ catalyst at 0 hr (bottom) and 24 hr (top) *dmso-d_6*. The reaction was performed at room temperature without the presence acetonitrile solvent with 5 mol% catalyst and 5 mmol TBHP under N_2 atmosphere.

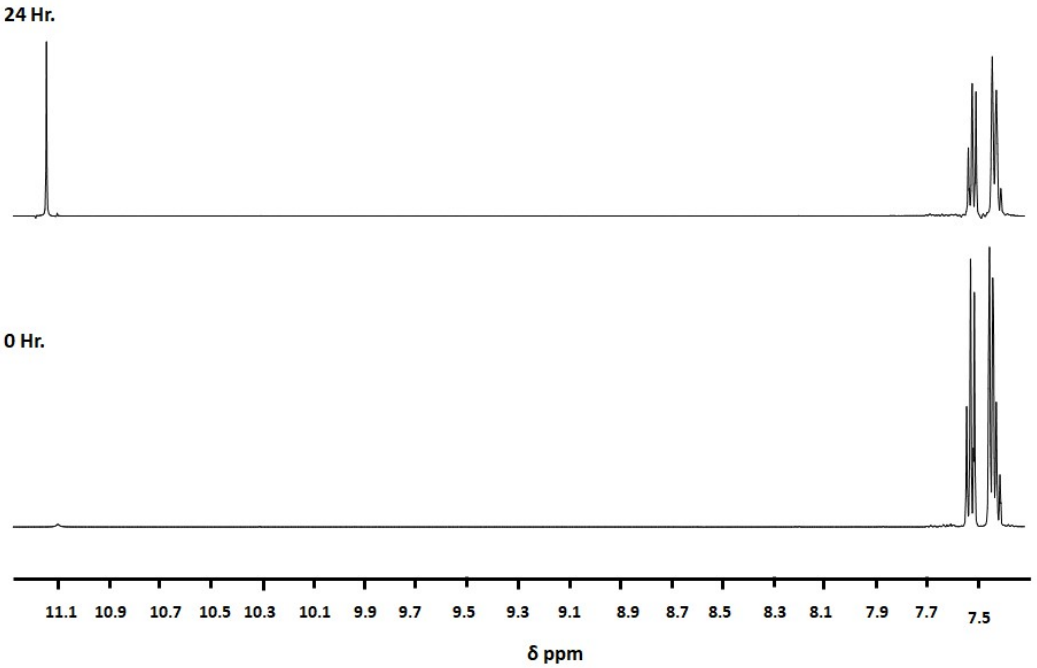

Fig. S24. Stacked ^{1}H NMR spectra of the reaction mixture of toluene to benzaldehyde in the presence of **$C_{10}H_{14}MoO_6$ [$MoO_2(acac)_2$]** catalyst at 0 hr (bottom) and 24 hr (top) in *dmso-d_6*. The reaction was performed at room temperature without the presence acetonitrile solvent with 5 mol% catalyst and 5 mmol TBHP under N_2 atmosphere.

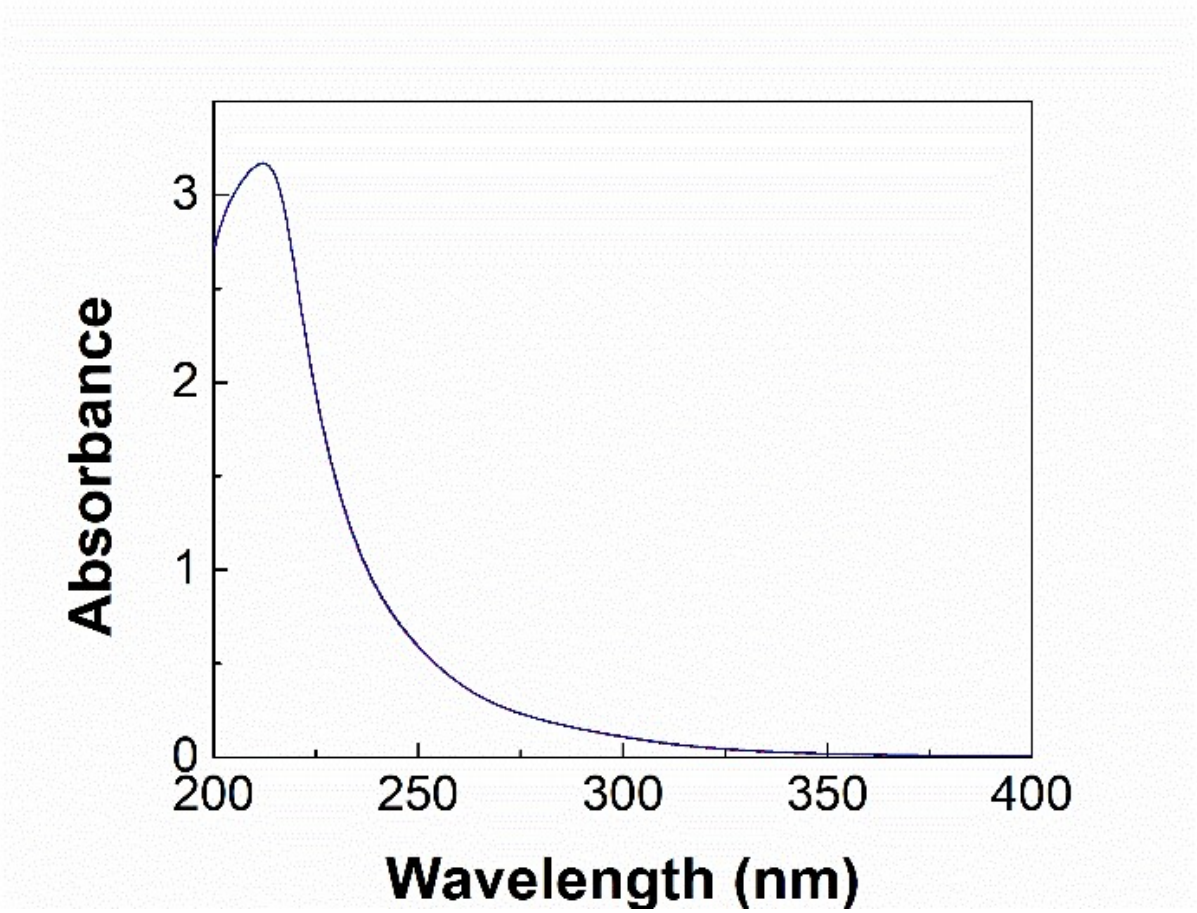

Fig. S25. Absorption spectra of **Ammonium molybdate $(NH_4)_6Mo_7O_{24}\cdot 4\ H_2O$** in acetonitrile solvent at 25 °C in the presence of NBT and TBHP at different time intervals is showing no significant reduction in absorption intensity of NBT at λ_{max} = 212 nm over the period of 50 min. Concentrations [NBT] = 14 × 10^{-6} M, **$(NH_4)_6Mo_7O_{24}\cdot 4\ H_2O$** = 4 × 10^{-6} M, [TBHP] = 13.75 × 10^{-5} M in ACN at 25 °C.

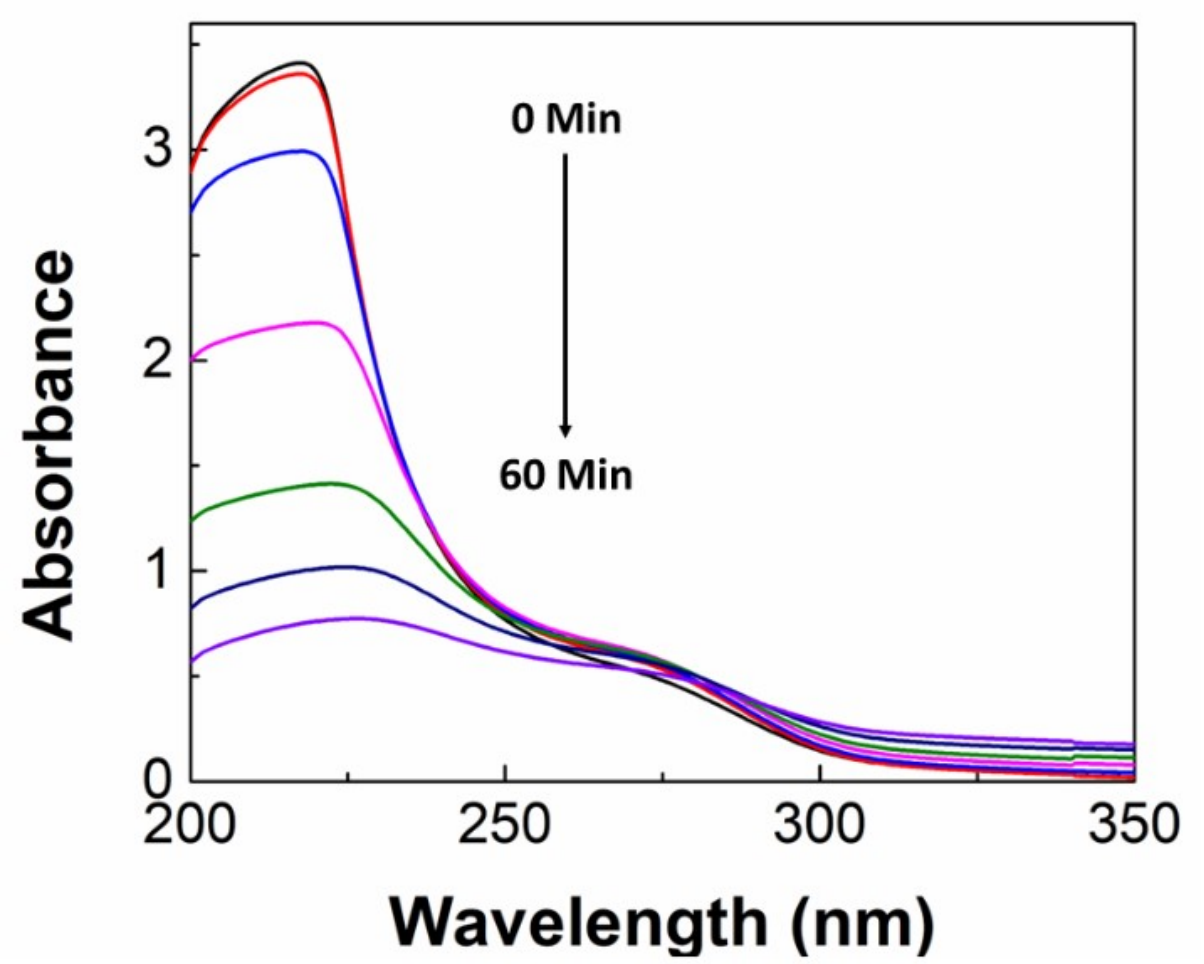

Fig. S26. Absorption spectra of **[$MoO_2(acac)_2$]** in acetonitrile solvent at 25 °C in the presence of NBT and TBHP at different time intervals showing a reduction in absorption intensity of NBT at λ_{max} = 217 nm over the period of 60 min. Concentrations [NBT] = 18 × 10^{-6} M, **[$MoO_2(acac)_2$]** = 1.5 × 10^{-5} M, [TBHP] = 13.75 × 10^{-5} M in ACN at 25 °C.

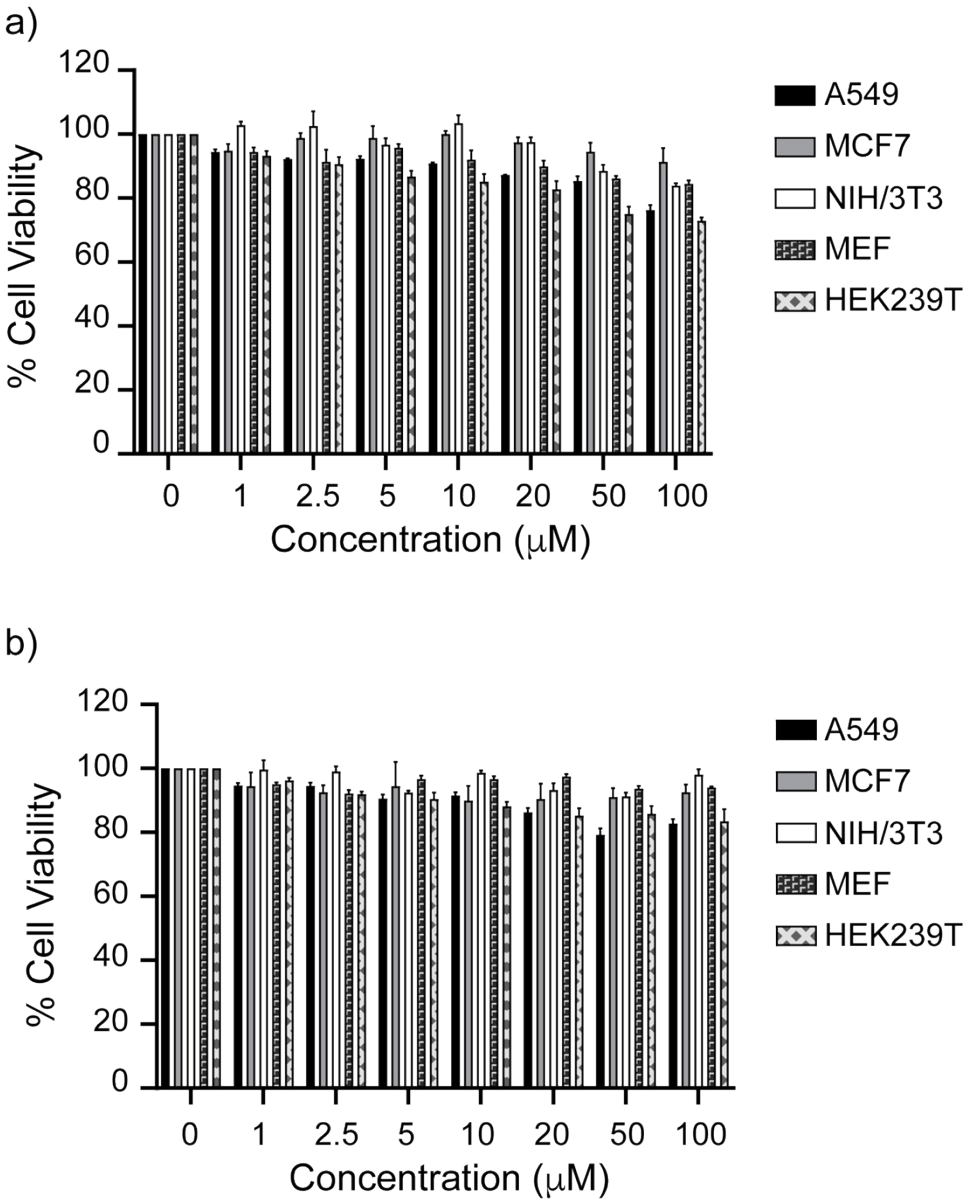

Fig. S27. Effect of a) maltol; and b) ammonium heptamolybdate on cell viability and growth in A549, MCF7, NIH/3T3, MEF, HEK 293T cells measured by MTT assay. The cells were treated with different concentrations of the test compound for 24 h and then cell viability was calculated by MTT assay. Data reported as the mean ± SEM for N = 4.

6. Computational Studies

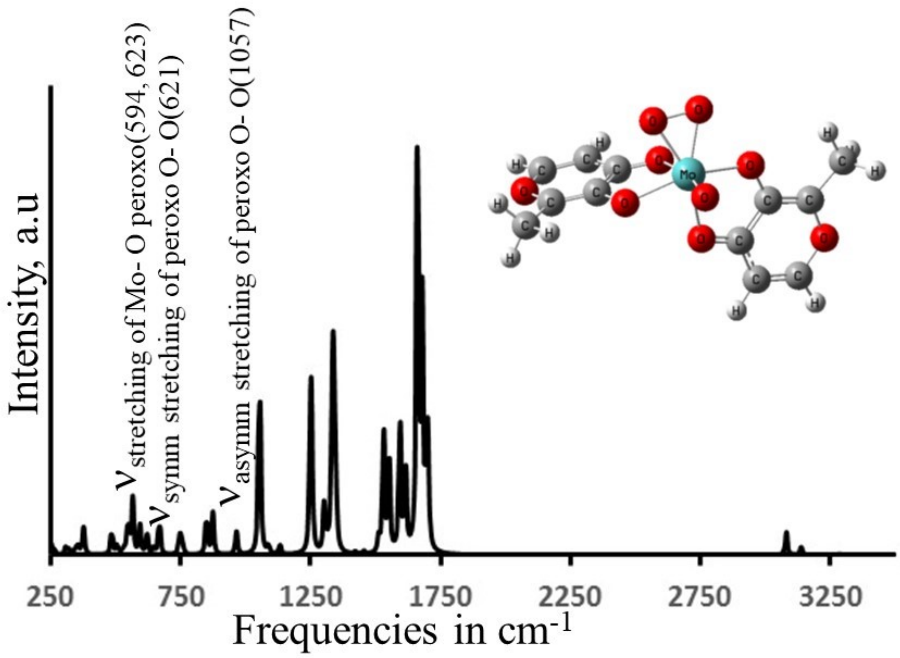

Fig. S28. The computed the IR frequencies for peroxo-Molybdenum complex. The Peroxo based vibrations are highlighted in the figure.

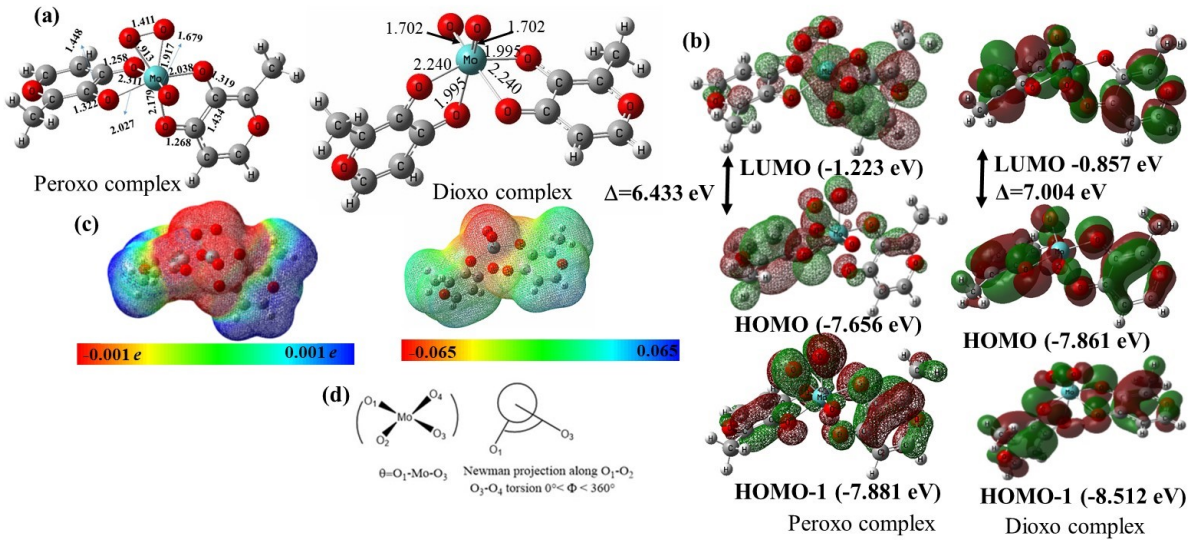

Fig. S29. (a) Optimized geometry with important bond distances in Å, (b) Frontier molecular orbitals (c) Molecular electrostatic potential map (isocontour value 0.002 eV/bohr^2) and (d) the definition of dihedral angle calculation of Mo(VI) peroxo complex.

Fig. S29 illustrates the Mo(VI)-peroxo compound optimization. This figure reveals that molybdenum coordinates with six ligands in a distorted octahedral environment, with two maltol rings twisted to accommodate two axial oxo and peroxo groups. We found that peroxo group coordinated to molybdenum with 1.91 Å distance where both oxygens are bonded with a length of 1.41 Å. The computed IR frequency confirms the formation of bond between the peroxo and Molybdenum group. The computed IR plots are given in the **Fig. S28.**

We calculated two angles, as reported by Webster and Hall in their study of DMSO reductase: (i) the largest angle subtended at the metal by two oxygen atoms from different ligands (θ= O_1-Mo-O_3) and (ii) the torsion angle made by the four oxygen atoms with the two oxygen atoms as the central atoms, as shown in the Newman projection formula in **Fig. S29**.[5] The proposed molybdenum structure exhibits a distorted octahedral structure with angular arrangements, with θ values of 83.98˚ and 78.21 ˚ and ϕ values of 97.91˚, which is lower than the dioxo compound **1** (θ = 155.76˚ and 79.50 ˚, and ϕ 164.39 ˚) values respectively. This shows that peroxo coordination increased the asymmetry in the structure. We also calculated the fold angles, as pointed out by Lauher and Hoffmann for metal dithiolene complexes, to help understand the oxidation state of the molybdenum.[6] The Mo(VI) oxidation state, the empty d^0-orbital results in a folded maltol ring with an angle of 2.2 °, which shows the planarity of the five member rings structure. The lower fold angle due to the larger electronegative of maltol groups which are not overlapping with metal d-orbitals. The frontier orbitals indicate that the ligand out-of-plane π orbitals (HOMO, HOMO-1) are delocalized with the π-donor oxo group where the metal contribution is minimal. The asymmetry shows that the peroxo compound MO orbital is not uniformly distributed on both side of the five-member ring while it is completely symmetry in the dioxo compound. However, the M-O-C-C-O metallocycle is planar in both dioxo and peroxo complexes, minimizing the filled-filled interaction between the ligand's out-of-plane orbitals and the metal in-plane orbitals. The computed molecular electrostatic potential map shows that the charge is completely delocalized on both rings, with negative charge accumulating at the axial ligands. The negative charge accumulation is more in peroxo compound owing to the relative more contribution from the metal centre.

The computation shows that peroxo can form a stable complex with Mo(VI) and the synthesised structure is similar to the reported and synthesized active site model of Molybdenum dithiolene complexes. The larger electronegativity of the maltol ligand made the structure more planar and delocalised with minimal contribution from metal atom compared to dithiolene counterpart.

7. References

1 W. L. F. Armarego and C. L. . Chai, *Purification of Laboratory Chemicals*, Elsevier, 6th Edition., 2009.

2 B. T. Cho, S. K. Kang, M. S. Kim, S. R. Ryu and D. K. An, *Tetrahedron*, 2006, **62**, 8164–8168.

3 M. J. Mintz and C. Walling, *Org. Synth.*, 1969, **49**, 9.

4 M.J. Frisch, et al., Gaussian 09 (Revision C.02), Gaussian, Inc., Wallingford, CT, 2009.

5 C.E. Webster, and M. B. Hall, *J. Am. Chem. Soc.* 2001, **123**, 5820.

6 J. W. Lauher, and R. Hoffmann, *J. Am. Chem. Soc.* 1976, **98**, 7, 1729–1742.